





8 | Parasitology | Research Article

Generation of inositol polyphosphates through a phospholipase C-independent pathway involving carbohydrate and sphingolipid metabolism in *Trypanosoma cruzi*

Mayara S. Bertolini,¹ Sabrina E. Cline,¹ Miguel A. Chiurillo,^{1,2} Brian S. Mantilla,^{1,3} Aharon Eidex,¹ Logan P. Crowe,¹ Danye Qiu,⁴ Henning J. Jessen,⁴ Adolfo Saiardi,⁵ Roberto Docampo¹

AUTHOR AFFILIATIONS See affiliation list on p. 24.

ABSTRACT Inositol phosphates are involved in a myriad of biological roles and activities such as Ca2+ signaling, phosphate homeostasis, energy metabolism, and disease pathogenicity. In Saccharomyces cerevisiae, synthesis of inositol phosphates occurs through the phosphoinositide phospholipase C (PLC)-catalyzed hydrolysis of phosphatidylinositol 4,5-bisphosphate (PIP2) into inositol 1,4,5-trisphosphate (IP3) and diacylglycerol and further IP3 phosphorylation by additional kinases that leads to the formation of highly phosphorylated inositol derivatives, known as inositol pyrophosphates. Inositol-tetrakisphosphate 1-kinase (ITPK1) is an enzyme that mediates a PLC-independent inositol polyphosphate synthesis through phosphorylation of inositol monophosphates and other intermediates in the cytosol. In this work, we identified and characterized a Trypanosoma cruzi ITPK1 (TcITPK1) homolog. The ability of TcITPK1 to act as the mediator for this alternative pathway was established through $plc1\Delta$ and $plc1\Delta$ isc1Δ yeast complementation assays and SAX-HPLC analyses of radioactively labeled inositol. TcITPK1 localizes to the cytosol, and knockout attempts of TcITPK1 revealed that only one allele was replaced by the DNA donor cassette at the specific locus, suggesting that null alleles may have lethal effects in epimastigotes. Ablation of T. cruzi phosphoinositide phospholipase C 1 (TcPI-PLC1) affected the synthesis of IP3 from glucose 6-phosphate but did not affect the synthesis of inositol polyphosphates, while ablation of inositol phosphosphingolipid phospholipase (TcISC1) affected the synthesis of inositol polyphosphates, thus revealing that the PLC-independent pathway using either glucose 6-phosphate or inositol phosphoceramide is involved in the synthesis of inositol polyphosphates, while the PLC-dependent pathway is involved in IP3 formation needed for Ca²⁺ signaling.

IMPORTANCE Millions of people are infected with *Trypanosoma cruzi*, and the current treatment is not satisfactory. Inositol pyrophosphates have been established as important signaling molecules. Our work demonstrates the presence of a phospholipase C-independent pathway for the synthesis of inositol pyrophosphates in *T. cruzi*. Furthermore, we demonstrate that this pathway starts with the synthesis of inositol monophosphates from glucose 6-phosphate or from inositol phosphoceramide, linking it to carbohydrate and sphingolipid metabolism. The essentiality of the pathway for the survival of *T. cruzi* infective stages makes it an ideal drug target for treating American trypanosomiasis.

KEYWORDS *Trypanosoma cruzi*, inositol pyrophosphates, phospholipase C, sphingolipids, inositol phosphoceramide

Invited Editor Igor C. Almeida, The Border Biomedical Research Center, El Paso, Texas, USA

Editor L. David Sibley, Washington University in St. Louis School of Medicine, St. Louis, Missouri, USA

Address correspondence to Roberto Docampo, rdocampo@uga.edu.

The authors declare no conflict of interest.

See the funding table on p. 24.

Received 25 October 2024 Accepted 4 March 2025 Published 2 April 2025

Copyright © 2025 Bertolini et al. This is an openaccess article distributed under the terms of the Creative Commons Attribution 4.0 International license.

Trypanosoma cruzi is an intracellular parasite and the causative agent for Chagas disease in humans. This is a zoonotic infection endemic to the Americas that currently affects 6–7 million individuals (1) and can infect many animal species. This parasite belongs to the eukaryotic supergroup Discoba, which is highly divergent from the Opisthokonta supergroup, which includes animals and fungi (2). Although some basic aspects of metabolism could be similar, each eukaryotic supergroup evolved independently and has unique characteristics that could be exploited for developing ways to eliminate the parasite without affecting its host. A case in point is the inositol phosphate pathway that is conserved in trypanosomes but with peculiarities not seen in animal cells.

Inositol phosphates regulate a large number of cellular functions such as Ca2+ signaling, energy metabolism, and phosphate homeostasis (3). The precursor of inositol phosphates in trypanosomes, myo-inositol, can be acquired from the extracellular medium via an inositol symporter (4-7) or synthesized endogenously (8, 9). Another potential source is by salvage of lipids from the host cells and remodeling in the mammalian stages, as occurs in Leishmania spp. (10, 11). Once inside the cells, inositol combines with CDP-diacylglycerol to form phosphatidylinositol (PI) in a reaction catalyzed by a phosphatidylinositol synthase (PIS). PI is phosphorylated by a PI kinase to form phosphatidylinositol phosphate (PI-4-P or PIP), and a PIP kinase (PIPK) generates phosphatidylinositol 4,5-bisphosphate (PIP2) (Fig. 1). The route for synthesis of inositol phosphates described in budding yeast (S. cerevisiae) involves the action of a phospholipase C (PLC) on PIP₂ releasing inositol 1,4,5-trisphosphate (IP₃) and diacylglycerol (12) (Fig. 1). IP₃ has a well-studied receptor, the IP₃ receptor, which participates in Ca²⁺ release from intracellular stores such as the endoplasmic reticulum (ER) in many eukaryotes (13). However, this receptor is found in acidocalcisomes of trypanosomes (14, 15). IP₃ can be further phosphorylated in mammals, trypanosomes, and S. cerevisiae at different hydroxyl positions producing IP₄ and IP₅ by inositol phosphate multikinase (IPMK; known as Arg82 in budding yeast) and IP₆ by inositol pentakisphosphate kinase (IPPK; known as lpk1 in yeast), producing the fully phosphorylated form known as inositol hexakisphosphate (IP₆), or phytic acid (Fig. 1). IP₅ and IP₆ can be the precursors of diphosphoinositol phosphates (PP-IPs, or simply IP7, IP8), also called inositol pyrophosphates (16). Inositol pyrophosphates are characterized by the presence of single (PP-IP4 and PP-IP₅) or double (PP₂-IP₃ and PP₂-IP₄) pyrophosphate moieties linked at different positions of the myo-inositol core (17). In trypanosomes, the biosynthesis of IP7 takes place by the action of inositol hexakisphosphate kinase (IP6K; known as Kcs1 in yeast) using IP₆ as the substrate and ATP as the phosphate donor (18, 19) (Fig. 1). Our molecular and physiological studies done with the phosphate/sodium symporters of T. brucei acidocalcisomes (TbPho91) and yeast vacuoles (Pho91p) demonstrated that IP7 interacts with their SPX domains, and this is essential for phosphate release to the cytosol (20). Therefore, IP₇ has been proposed as a signaling molecule in trypanosomes with critical importance in phosphate homeostasis.

In mammalian cells (21), *S. cerevisiae* (22), and trypanosomes (6), in addition to its uptake from the extracellular medium, *myo*-inositol can be generated endogenously by isomerization of glucose 6-phosphate (G6P) into inositol 3-phosphate (3-IP₁), catalyzed by the inositol 3-phosphate synthase (known as INO1 in yeast and ISYNA1 in mammals). In mammalian cells, 3-IP₁ can be further phosphorylated by the inositol tetrakisphosphate 1-kinase 1 (ITPK1) (22, 23) to produce substrates for other inositol phosphate kinases such as IPMK and IPPK and generate IP₆ and inositol pyrophosphates (Fig. 1). An alternative PLC-independent pathway discovered in yeast PLC *null* mutants transformed with *HsITPK1* could potentially utilize endogenous inositol generated from inositolphosphoceramide (IPC) (22), a highly abundant sphingolipid in trypanosomes, fungi, and plants but absent in mammals, as a substrate for ITPK1 (Fig. 1). In mammalian cells, ISYNA1 knockout cells are still capable of producing inositol polyphosphates, indicating the existence of an alternative endogenous pathway for their synthesis (24).

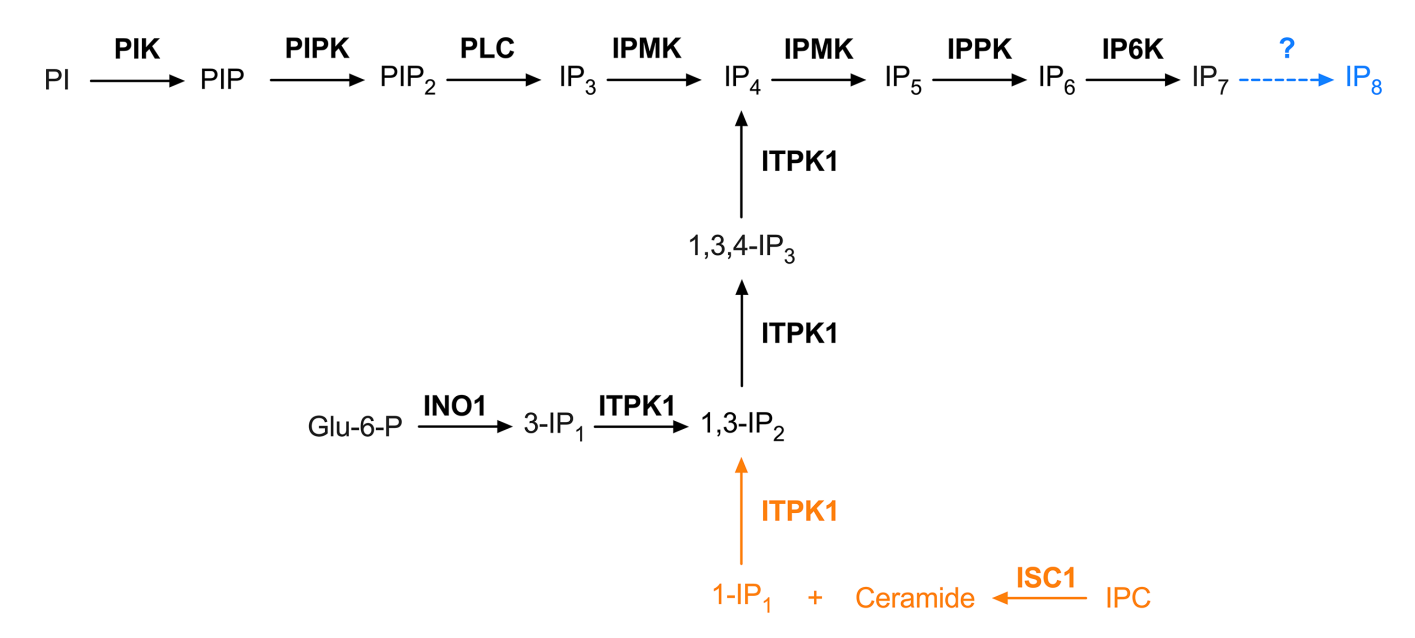


FIG 1 Synthesis of inositol pyrophosphates. Phosphatidylinositol (PI) is phosphorylated by a PI kinase (PIK) to form phosphatidylinositol phosphate (PI-4-P or PIP), and a PIP kinase (PIPK) generates phosphatidylinositol 4,5-bisphosphate (PIP₂). A phospholipase C (PLC) catalyzes the formation of inositol 1,4,5-trisphosphate (IP₃) from PIP₂ via the lipid route. IP₃ is further converted into inositol polyphosphates through kinase reactions catalyzed by inositol phosphate multikinase (IPMK), which forms inositol tetrakisphosphate (IP₄) and inositol pentakisphosphate (IP₅); inositol pentakisphosphate kinase (IPPK), which forms inositol hexakisphosphate (IP₆); and inositol hexakisphosphate kinase (IP6K), which forms diphosphoinositol pentakisphosphate (IP₇) and possibly bis-diphosphoinositol tetrakisphosphate (IP₈). Alternative routes (cytosolic routes) start with the conversion of glucose 6-phosphate to inositol 3-phosphate (3-IP₁) by inositol-3-phosphate synthase (INO1), followed by kinase reactions catalyzed by inositol tetrakisphosphate 1-kinase (ITPK1), or start with the formation of inositol 1-phosphate (1-IP₁) from inositol phosphoceramide (IPC) by inositol sphingolipid phospholipase C-like protein (ISCL), with further kinase reactions by ITPK1. Note that PLC produces inositol 1,4,5-trisphosphate, while the alternative pathways likely produce inositol 1,3,4-trisphosphate. The enzyme that catalyzes the conversion of IP₇ into IP₈ (blue) in *T. cruzi* is unknown. The pathway that converts IPC into 1-P₁ and ceramide (orange) is present in *T. cruzi* but absent in mammals.

In this work, we investigated the role of the PLC-dependent and PLC-independent pathways in the synthesis of inositol pyrophosphates in *T. cruzi*. Knockout of *T. cruzi* phosphoinositide phospholipase C 1 (*TcPl-PLC1*) revealed that the PLC-dependent pathway is not necessary for the synthesis of inositol polyphosphates, while TcITPK1 is required for their PLC-independent synthesis, using either glucose 6-phosphate or inositolphosphoceramide as a source of inositol monophosphate.

RESULTS

Characterization of TcITPK1

One gene (TcYC6_0083580; KAF8297109.1) encoding a putative inositol tetrakisphosphate 1-kinase 1 (TcITPK1) was found in the *T. cruzi* Y strain genome at the TriTryp and NCBI databases. The orthologs identified in the related trypanosomatids *T. brucei* (Tb927.8.290; XP_847459) and *Leishmania major* (LmjF.24.1930; XP_001683711.1) shared 39.7% and 21.9% amino acid identity, respectively, to TcITPK1, which shares 17.1% identity and 30.7% similarity with human ITPK1 (NP_001136065). The open reading frame predicts a protein of 419 amino acids with a molecular weight of 46.58 kDa.

ITPK1 is a conserved inositol phosphate kinase. Recent studies have demonstrated that *Lokiarchaeum candidatum* ITPK1 shares structural and homology similarities with *Homo sapiens* and *Entamoeba histolytica* ITPK1. Highly conserved residues at H167, K199, and R212 of HsITPK1 are located near the IP-contact residues and are proximal to the ATP-binding site (22). Additionally, these ITPK1 homologs share less conserved residues at K18, K59, H162, and G301 (22). A Clustal Omega multiple sequence alignment of previously established homologs, including sequences derived from the kingdoms

Plantae (*Oryza sativa* and *Zea mays*), Animalia (*Homo sapiens, Mus musculus, Gallus gallus,* and *Danio rerio*), Protista (*Dictyostelium discoideum, Entamoeba histolytica,* and *Monosiga brevicollis*), and Archaea (*Lokiarchaeum candidatus*) with the hypothetical protein found in *T. cruzi*, was completed to determine if the protein TcYC6_0083580 has the conserved inositol phosphate and ATP contact residues. The *T. cruzi* hypothetical protein was shown to share the H167 and K199 highly conserved HsITPK1 residues (H198 and K242 in TcITPK1) and a few of the less conserved HsITPK1 residues at K18, K59, and G301 (K20, K77, and G378 in TcITPK1) (Fig. S1). The CLUSTAL Omega alignment reinforces the hypothesis that the hypothetical protein TcYC6_0083580 is TcITPK1.

Once TcYC6_0083580 was established as a TcITPK1 ortholog, a phylogenetic tree was constructed to investigate the evolutionary relationships of the ITPK1 gene in kinetoplastid parasites and, by association, the PLC-independent inositol phosphate pathway (Fig. S2). The tree included several outgroup species, such as *Lokiarchaeum candidatus*, *Naegleria fowleri*, *Entamoeba histolytica*, and *Homo sapiens*, which were used to provide a clear evolutionary baseline for comparison with the kinetoplastid parasites. Within the kinetoplastid parasite branches, there is a strong evolutionary clustering of ITPK1, with most branches having bootstrap values above 80, indicating high statistical support for the relationships.

To define the cellular localization of TcITPK1, CRISPR/Cas9 endogenous C-terminal tagging of TcITPK1 with a 3×c-Myc tag was done (Fig. 2A) and verified by PCR (Fig. 2B shows predominant bands of 1,500 bp) and Western blot analysis (Fig. 2C). Immunofluorescence assays in epimastigotes localized this protein to the cytosol of the parasite (Fig. 2D).

AlphaFold-2.1.1 (25) was utilized to predict the structural conformation of TcITPK1 and HsITPK1. Both the relaxed (Fig. S3A and C) and unrelaxed (Fig. S3B and D) ribbon models demonstrate high structural confidence in the core of the proteins near the inositol phosphate-contact and ATP-binding site residues with per-residue model confidence score (pLDDT) values of greater than 90, denoted in dark blue. There are some lower confidence regions of the TcITPK1 protein structure (denoted by yellow and orange); however, this lower confidence score may be due to evolutionary diversity outside of ITPK1's catalytic site.

After three-dimensional resolution of TcITPK1 by AlphaFold-2.1.1, the model was analyzed by COFACTOR (26, 27) to glean structural-based function predictions for ligand-binding partners and ligand-binding sites. COFACTOR predicted that IP₃ would bind to TcITPK1 at residues K20, T192, G193, H198, K242, Y244, Q277, N374, P377, and G378 (Fig. S3E). Additionally, the predicted TcITPK1 model with IP₃ was structurally aligned with the HsITPK1 model using TM-align parameters on RCSB PDB (Fig. S3F).

The AlphaFold-2.1.1-predicted TcITPK1 model was also compared to the X-ray diffracted HsITPK1 (PDB: 2ODT) using the pairwise structural alignment tool (28–35). Both ITPK1 proteins had highly conserved secondary structures and minor spatial modulation of alpha-helical structures (Fig. S3G). Additionally, when comparing TcITPK1 with HsITPK1 (PDB: 2ODT), the two structures were found to have 272 equivalent positions with a root mean square deviation (RMSD) of 3.05 Å without twists, denoting strong alignment between the eukaryotic orthologous ITPK1 structures. The 0.57 TM-score demonstrated a similar protein structure between AlphaFold-2.1.1-TcITPK1 and HsITPK1 (PDB: 2ODT). Further structural studies are warranted.

Functional validation *in vivo* of the role of TcITPK1 in the synthesis of inositol polyphosphates

We investigated the activity of *T. cruzi* ITPK1 *in vivo* by transforming *S. cerevisiae* strains with different genetic backgrounds: wild-type (BY4741), *PLC1*-ablated ($plc1\Delta$), and *PLC1*-and *ISC1*-ablated ($plc1\Delta$ isc1 Δ). The goal was to assess the production of IP₆ (the most abundant inositol polyphosphate), IP₇, and IP₈. The $plc1\Delta$ strain was used to prevent IP₆ formation through the yeast PLC1 pathway as PLC1 is the only pathway in yeast responsible for IP₆ synthesis (22). In addition, it has been reported that in yeasts, degradation of

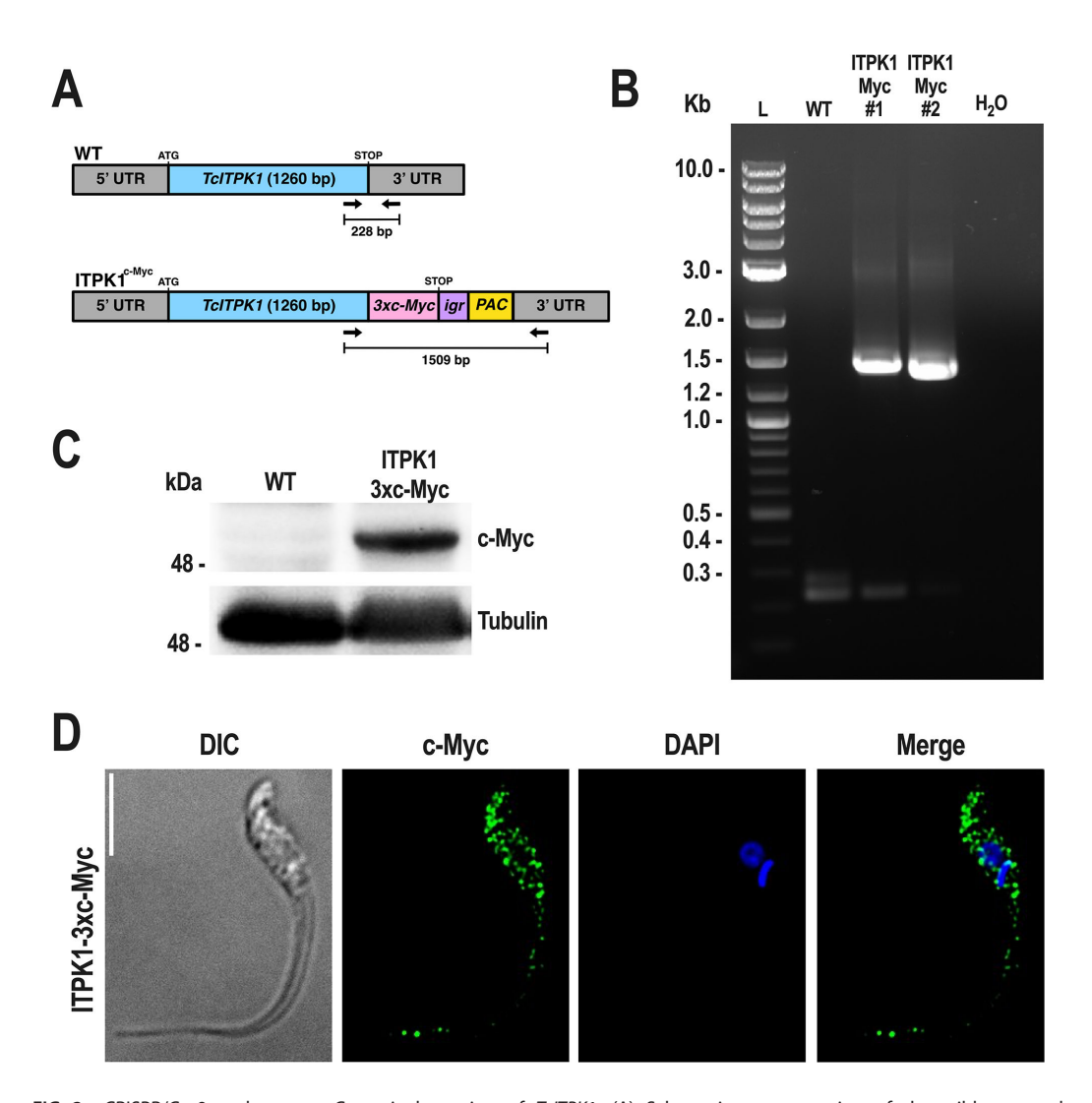


FIG 2 CRISPR/Cas9 endogenous C-terminal tagging of TcITPK1. (A) Schematic representation of the wild-type and endogenous tagged TcITPK1 gene. Epimastigotes were endogenously tagged with a 3xc-Myc tag using CRISPR/Cas9 genome editing. (B) PCR analysis for validation of TcITPK1 tagging showing expected bands for control cell lines (predicted size, 228 bp) and TcITPK1-3xc-Myc cell line (predicted size, 1,509 bp). Lanes: L, 1 kb plus ladder; WT, wild-type; ITPK Myc#1, TcITPK1-3xc-Myc#1; ITPKMyc#2, TcITPK1-3xc-Myc #2; H₂O, PCR negative control. Clone#1 was selected for further study as clone#2 was smaller. (C) Western blot analysis of wild-type and TcITPK1-3xc-Myc epimastigotes using the monoclonal antibody against c-Myc tag. The predicted protein molecular mass for TcITPK1-3xc-Myc is 50.9 kDa. Molecular markers are on the left. Tubulin was used as a loading control. (D) Localization of endogenously tagged TcITPK1-3xc-Myc in epimastigotes using anti-c-Myc antibodies. DIC, differential interference contrast. c-Myc (green), TcITPK1-3xc-Myc. The merge image shows TcITPK1-3xc-Myc (green) and DAPI staining (blue). Scale bar = 5 μ m.

IPC by inositol phosphosphingolipid phospholipase (known as ISC1 in yeast) generates ceramide and inositol 1-phosphate (1-IP₁) (Fig. 1). 1-IP₁ can be a substrate for HsITPK1 in yeasts lacking PLC1 (22). Human ITPK1 was used as a positive control, while strains transformed with an empty vector served as negative controls. We also included two TcITPK1 mutants, H198A and K242A, both of which are predicted to disrupt its activity, for transformation. Successful plasmid incorporation and protein expression were confirmed by PCR (Fig. S4A) and immunofluorescence assays, respectively (Fig. S4B).

We tested the growth of these strains on normal SC-URA medium or medium without inositol (Fig. 3A) and found that the growth of all strains in the medium with inositol was normal regardless of whether they were transformed with the empty plasmid, HsITPK1, or TcITPK1. This indicates that external inositol compensates for any disruptions in

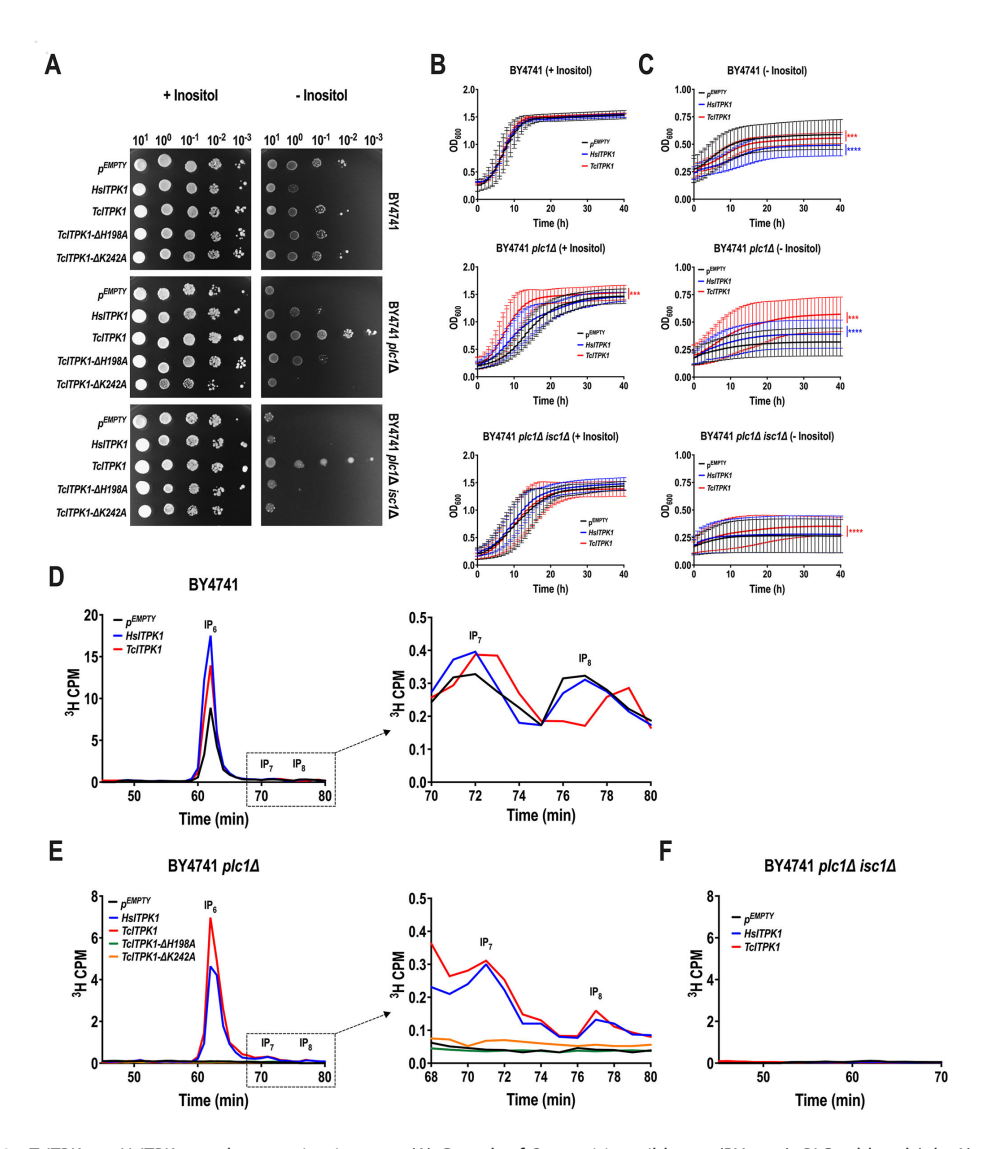


FIG 3 TcITPK1 or HsITPK complementation in yeast. (A) Growth of S. cerevisiae wild-type (BY4741), PLC1-ablated ($plc1\Delta$), and PLC1- and ISC1-ablated ($plc1\Delta$) transformed with the empty vector pCA45 (pEMPTY), pCA45-HsITPK1, or pCA45-HsITPK1, in liquid SC-URA medium with (B) or without (C) HsITPK1, or pCA45-HsITPK1, or pCA45-HsITPK1, in liquid SC-URA medium with (B) or without (C) HsITPK1, or pCA45-HsITPK1, or pCA45-HsITPK1, or pCA45-HsITPK1, or a total period of 40 hours. Values are expressed as means HsITPK1, red asterisks = pEMPTY vs HsITPK1; red asterisks = pEMPTY vs HsITPK1. (D) SAX-HPLC analysis of IPs from the [HsITPK1] (red line). (E) SAX-HPLC analysis of IPs from the [HsITPK1] (red line), pCA45-HsITPK1 (blue line), or pCA45-HsITPK1 (blue line),

inositol phosphate metabolism caused by the transformations. In contrast, on agar plates without inositol, the growth patterns varied. The wild-type strain exhibited impaired-to-partially normal growth when transformed with either HsITPK1 or TcITPK1, suggesting that these kinases may disrupt inositol phosphate metabolism under inositol-depleted conditions. The $plc1\Delta$ strain showed impaired growth with the empty plasmid, but

growth was restored to partially normal levels with TcITPK1, indicating a compensatory effect by this kinase. Conversely, the $plc1\Delta$ $isc1\Delta$ strain displayed generally impaired growth across all conditions, although TcITPK1 provided some improvement. These results suggest that inositol phosphate metabolism is significantly affected by the absence of PLC1 and ISC1, with TcITPK1 offering compensation in the absence of inositol, whereas HsITPK1 does not alleviate the growth impairment as effectively. We also tested the growth of these strains in liquid SC-URA media with and without inositol, and the results were consistent with those observed on agar plates (Fig. 3B and C).

We assessed the impacts of ITPK1 complementation using SAX-HPLC analysis with [3 H]inositol labeling to quantify the formation of inositol phosphate species. Both TcITPK1 and HsITPK1 could complement yeast deficient in IP $_6$ formation, functionally validating the activity of these enzymes *in vivo* (Fig. 3D and E). Interestingly, both human and T. cruzi ITPK1 increased (above normal) the level of IP $_6$ in the wild-type background (Fig. 3D). When TcITPK1 mutated in amino acids H198A and K242A, predicted to be part of the catalytic site, was used for transformation of $plc1\Delta$ yeast, no rescue was observed (Fig. 3E). In contrast to the results obtained in yeast $plc1\Delta$ mutants, in the $plc1\Delta$ isc1 Δ strain, the level of IP $_6$ was not rescued by either human or TcITPK1 (Fig. 3F), demonstrating that inositol derived from sphingolipids could be used by both TcITPK1 and HsITPK1 to generate IP $_6$.

Attempts to knockout TcITPK1 gene expression

We designed a CRISPR/Cas9 strategy to generate KO mutants of this gene. The method involves the constitutive expression of Cas9 and specific single-guide RNA (sgRNA) and the utilization of a DNA donor template to promote double-strand break repair by homologous-directed repair (36). Two different cassettes were utilized along with two unique *TcITPK1*-targeted sgRNA designs. Each of the four unique designs was used in technical duplicates, and the complete co-transfection experiments were repeated a total of three independent times. Each of the transfections resulted in mixed populations of *TcITPK1*-ablated and WT epimastigotes. However, after limiting dilution to isolate *TcITPK1*-KO parasites, no epimastigotes survived the selection process, suggesting the essentiality of this gene for cell proliferation.

We then used a T7RNAP/Cas9 strategy to try to obtain TcITPK1-KO parasites. This cloning-free genome editing method involves co-transfecting a sgRNA template with a T7 promoter and donor DNA as PCR products (37). In addition, to generate a null mutant population using the T7RNAP/Cas9 system in a single round of electroporation, it is necessary to transfect cells with two donor DNAs, each one containing a different resistance marker (37). We employed a two-step approach: (i) first, we transfected T7RNAP/Cas9 epimastigotes with an sgRNA and one (PAC) or two (PAC and BSD) donor DNAs. (ii) If the knockout (KO) cell line was non-viable, a second transfection introduced the BSD cassette into a stable single-allele deletion mutant generated in the first round. We successfully generated a TcITPK1 single-knockout (TcITPK1-SKO) cell line as both attempts (transfecting with two resistance cassettes simultaneously or using two sequential rounds of transfections) failed to produce null mutant cells for this gene. This result was confirmed through PCR (Fig. 4A and B) and Southern blot analysis (Fig. 4C; Fig. S5A). In addition, the growth rate of TcITPK1-SKO epimastigotes was not affected as compared with cells transfected with scrambled sgRNA (Fig. 4D). Metacyclogenesis, studied by incubating epimastigotes in triatome artificial urine, was stimulated in TcITPK1-SKO cells (Fig. 4E). We then infected Vero cells with tissue culture-derived trypomastigote stages and measured both the ability of trypomastigotes to infect host cells (Fig. 4F) and the replication of intracellular amastigotes (Fig. 4G), as described in Materials and Methods. Both trypomastigote invasion and amastigote replication were significantly affected by single knockout of *TcITPK1*, compared to control cells.

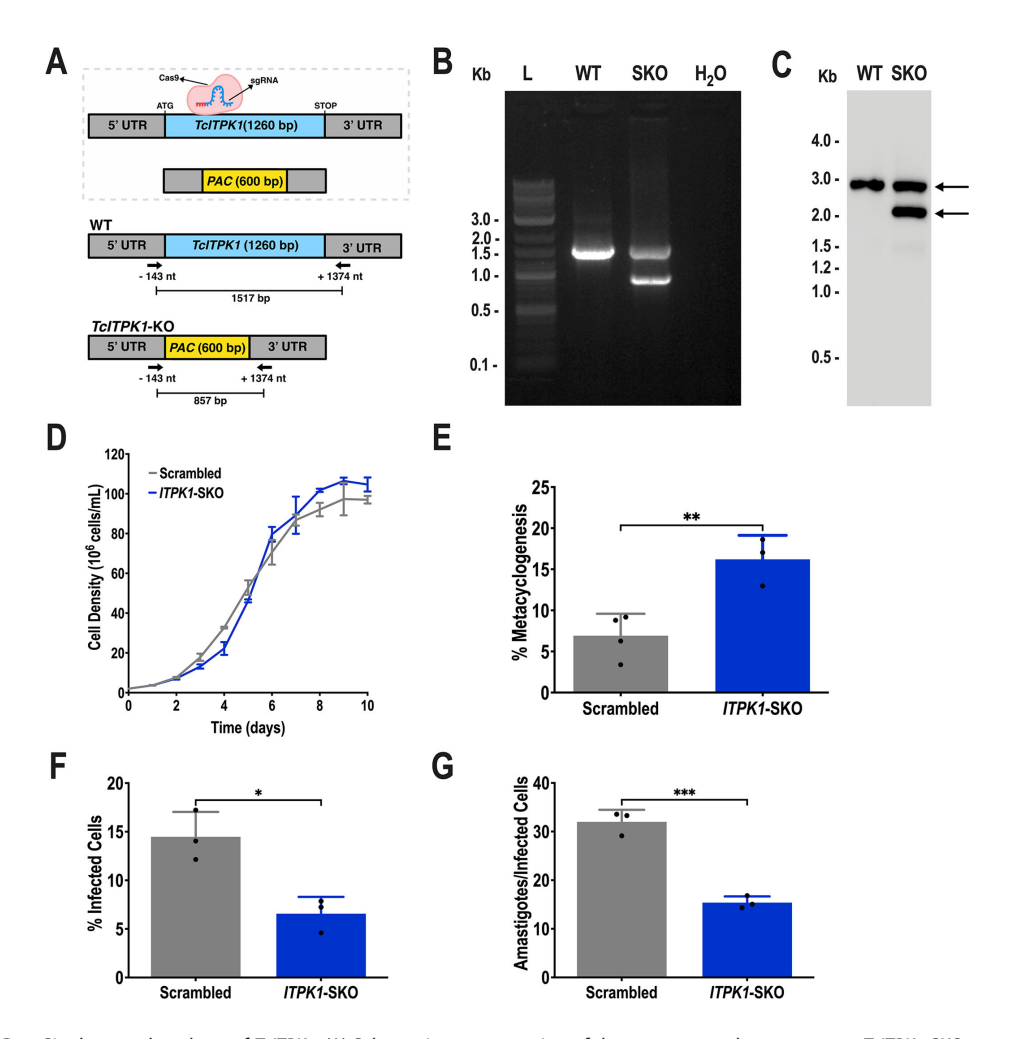


FIG 4 Single-gene knockout of *TcITPK1*. (A) Schematic representation of the strategy used to generate a *TcITPK1*-SKO mutant by homologous recombination and primers (arrows) used to verify gene replacement by PCR. The intact locus generates a PCR product of 1,517 bp, while the disrupted locus generates a fragment of 857 bp. (B) PCR analysis showing that a single gene of *TcITPK1* was ablated at its genomic locus and replaced in genomic DNA of the SKO cell line. Lanes: L, 1 kb plus ladder; WT, wild type; SKO, *TcITPK1*-SKO; H_2O , PCR negative control. (C) Southern blot analysis of wild-type and *TcITPK1*-SKO (SKO) gDNA digested with the Pvull restriction enzyme. The blot was hybridized with a biotin-labeled probe corresponding to 455 bp of *TcITPK1* 5' UTR (nt -729 to -275), revealing a 2,700 bp band for Pvull-digested gDNA from WT cells and a 2,040 bp band for Pvull-digested gDNA from *TcITPK1*-SKO cells (arrows). (D) Growth of control (scrambled) and *TcITPK1*-SKO (*ITPK1*-SKO) epimastigotes in the LIT medium. (E) Percentage of metacyclic trypomastigotes in epimastigote cultures after incubation in the TAU 3AAG medium. Differentiation of epimastigotes to metacyclic trypomastigotes was quantified by staining with DAPI to distinguish the position of the kinetoplast by fluorescence microscopy. Values are expressed as means \pm SD (n = 3) **P ≤ 0.01 by Student's t test. (F) *TcITPK1*-SKO trypomastigote infection of Vero cells at 4 hours post-infection was significantly inhibited. Values are expressed as means \pm SD (n = 3) **P ≤ 0.05 by Student's t test. (G) The number of intracellular amastigotes per infected host cell observed 48 hours post-infection was also significantly reduced. Values are expressed as means \pm SD (n = 3) ***P ≤ 0.001 by Student's t test.

Overexpression of TcITPK1 in T. cruzi cells

To complete the functional study of TcITPK1, we also evaluated the effects of its upregulation in different stages of the *T. cruzi* life cycle by generating a mutant cell line (*TcITPK1*-OE) overexpressing the full-length (1,260 aa) C-terminal tagged protein (TcITPK1-3×HA). We evaluated the expression of TcITPK1-3×HA in a clonal population by Western blot analysis using anti-HA antibodies. The high-molecular weight signal detected in total protein extracts of *TcITPK1*-OE parasites corresponds to the predicted size of TcITPK1-3×HA (~50 kDa) (Fig. 5A). Fluorescence microscopy images showed a

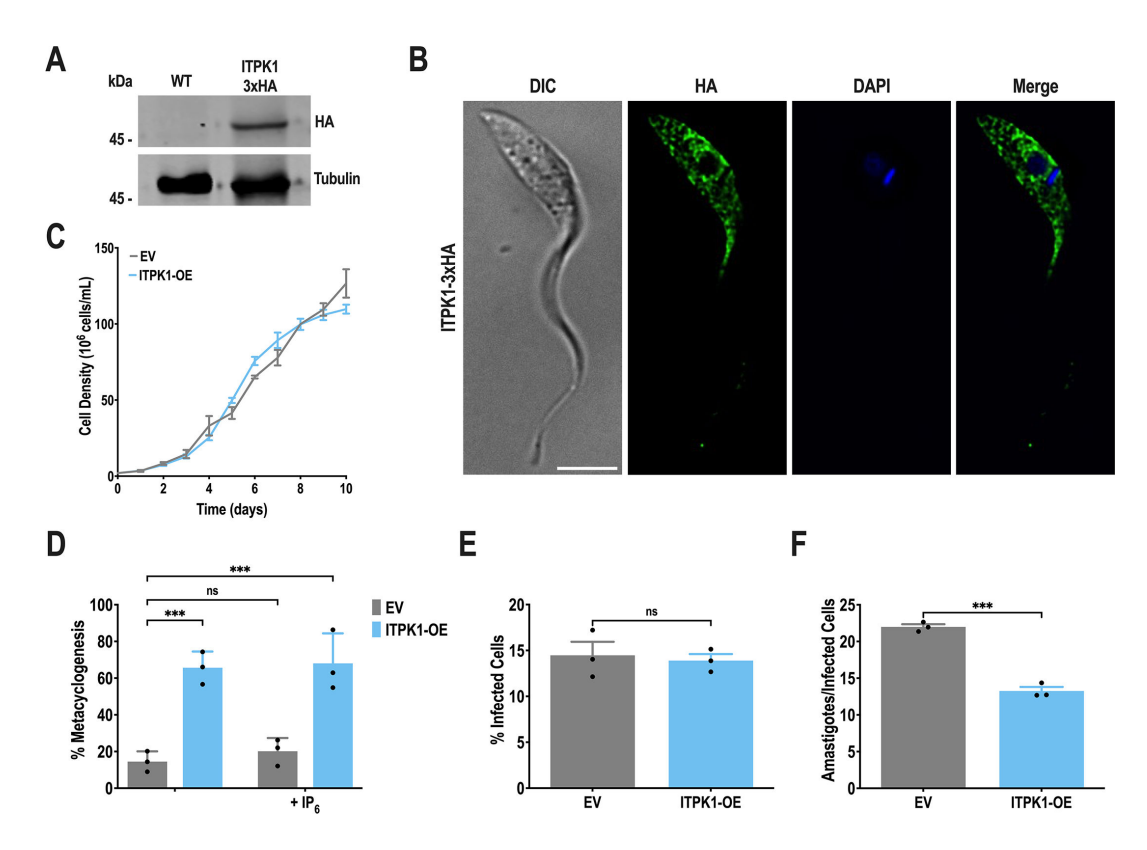


FIG 5 *TcITPK1* overexpression. (A) Western blot analysis of wild-type and TcITPK1-3×HA epimastigotes using monoclonal antibodies against the HA tag. The predicted protein molecular mass for TcITPK1-3×HA is 49 kDa. Molecular markers are on the left. Tubulin was used as a loading control. (B) Localization of TcITPK1-3×HA in epimastigotes using anti-HA antibodies. DIC, differential interference contrast. HA (green), TcITPK1-3×HA. The merge image shows TcITPK1-3×HA (green) and DAPI staining (blue). Scale bar = 5 µm. (C) Growth of control (EV, empty vector) and TcITPK1-3×HA (ITPK1-OE) epimastigotes in the LIT medium. (D) Percentage of metacyclic trypomastigotes in epimastigote cultures after incubation in the TAU 3AAG medium in the presence or absence of 150 µM IP₆. Values are expressed as means \pm SD (n = 3) **** $P \le 0.001$ by two-way ANOVA with Dunnett's multiple-comparison test. (E) TcITPK1-3×HA trypomastigote infection of Vero cells at 4 hours post-infection was not significant. Values are expressed as means \pm SD (n = 3) by Student's t = 0.001 to Student's t = 0.001 by Student's t = 0.001

localization pattern like that exhibited by the endogenous tagged protein (Fig. 5B). *TcITPK1*-OE epimastigotes had the same growth rate as control cells transfected with the pTREX-n empty vector (Fig. 5C). Notably, *TcITPK1*-OE exhibited a significantly increased capacity to differentiate *in vitro* into metacyclic trypomastigotes (Fig. 5D). Moreover, the ability of trypomastigotes to infect host cells was not affected (Fig. 5E), while the replication of intracellular amastigotes was significantly impaired by overexpression of *TcITPK1*, compared to control cells (Fig. 5F).

Phospholipase C knockout in *T. cruzi* does not affect the synthesis of inositol polyphosphates

To explore the role of phospholipase C in inositol polyphosphate synthesis, we designed a CRISPR/Cas9 strategy to generate KO mutants of this gene (Fig. 6A). After 5 weeks of selection with G418 and blasticidin, knockout of *TcPl-PLC1* was validated by PCR (Fig. 6B) and, after cloning by limiting dilution, by Southern blot analysis using probes comprising the 5' end and the 5' UTR (Fig. 6C and D; Fig. S5B).

Proliferation of epimastigotes was slightly stimulated in stationary-phase *TcPI-PLC1*-KO parasites either in the presence of regular (Fig. 6E) or low glucose levels (Fig. 6F). *TcPI-PLC1*-KO cells were able to differentiate to metacyclic trypomastigotes in a higher proportion than control cells (Fig. 6G). Furthermore, *TcPI-PLC1* knockout had a significant

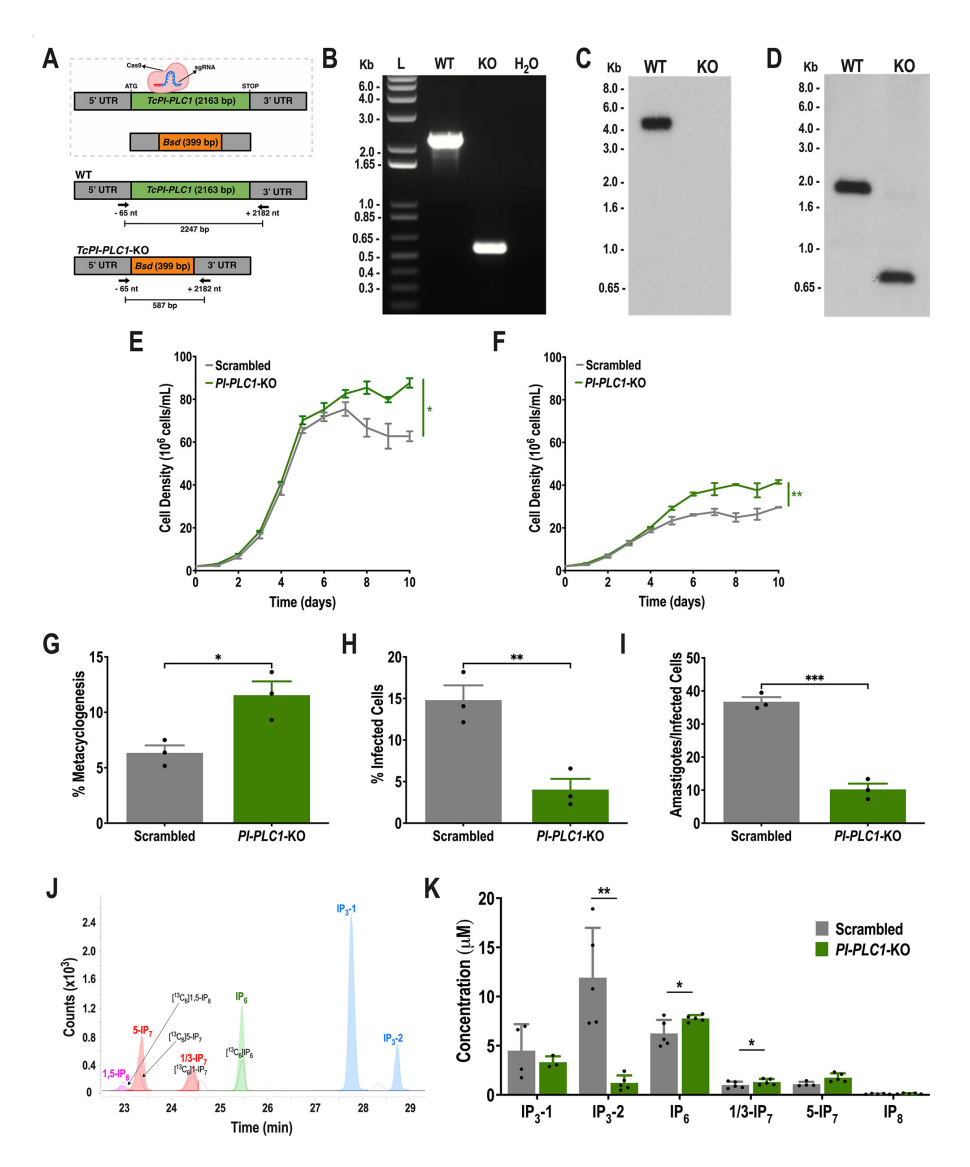


FIG 6 Knockout of TcPI-PLC1. (A) Schematic representation of the strategy used to generate a TcPI-PLC1-KO mutant by homologous recombination and primers (arrows) used to verify gene replacement by PCR. The intact locus generates a PCR product of 2,247 bp, while the disrupted locus generates a fragment of 587 bp. (B) PCR analysis showing that TcPI-PLC1 was ablated at its genomic locus and replaced in genomic DNA of the KO cell line. Lanes: L, 1 kb plus ladder; WT, wild-type; KO, TcPI-PLC1-KO; H₂O, PCR-negative control. (C) Southern blot analysis of wild-type and TcPI-PLC1-KO (KO) gDNA digested with the BamHI restriction enzyme. The blot was hybridized with a ³²P-labeled probe corresponding to 439 bp of *TcPI-PLC1* (nt +1 to +439), revealing a 4,419-bp band only for BamHI-digested gDNA from WT cells. (D) Southern blot analysis of wild-type and TcPI-PLC1-KO (KO) gDNA digested with the Pvull restriction enzyme. The blot was hybridized with a ³²P-labeled probe corresponding to 460 bp of TcPI-PLC1 5' UTR (nt -503 to -1), revealing a 1,628-bp band for Pvull-digested gDNA from WT cells and a 715 bp band for Pvull-digested gDNA from TcPI-PLC1-KO cells. (E) Growth of control (scrambled) and TcPl-PLC1-KO (Pl-PLC1-KO) epimastigotes in the LIT medium. Values are expressed as means \pm SD (n = 3) *P ≤ 0.05 by Student's t test. (F) Growth of control (scrambled) and TcPI-PLC1-KO (PI-PLC1-KO) epimastigotes in low-glucose LIT medium. Values are expressed as means \pm SD (n = 3) ** $P \le 0.01$ by Student's t test. (G) Percentage of metacyclic trypomastigotes in epimastigote cultures after incubation in the TAU 3AAG medium. Values are expressed as means \pm SD (n=3) * $P \le 0.01$ by Student's ttest. (H) TcPI-PLC1-KO trypomastigote infection of Vero cells at 4 hours post-infection was significantly reduced. Values are expressed as means \pm SD (n = 3) ** $P \le 0.01$ by Student's t test. (I) The number of intracellular amastigotes per infected host cell observed 48 hours post-infection was also significantly reduced. Values are expressed as means \pm SD (n=3) *** $P \le$ 0.001 by Student's t test. (J, K) Inositol phosphate extraction from scrambled and TcPI-PLC1-KO (PI-PLC1-KO) parasites, followed by CE-ESI-MS analysis, enables the identification of several important inositol phosphate and pyrophosphate isomers. (J) (Continued on next page)

Fig 6 (Continued)

Separation of inositol phosphates by CE-ESI-MS from a *TcPI-PLC1*-KO sample. Black line: extracted ion electropherograms of $[^{13}C_6]$ 1–5-IP₈, 5-IP₇, 1/3-IP7, and IP₆ references; pink line: extracted electropherograms of IP₈ in the sample; red line: extracted ion electropherograms of IP₆ in the sample; green line: extracted ion electropherograms of IP₆ in the sample; blue trace: extracted ion electropherograms of IP₃ in the sample. (K) Concentration of inositol phosphates in scrambled and *TcPI-PLC1*-KO (*PI-PLC1*-KO) cells by CE-ESI-MS analysis shows that synthesis of IP₆ and IP₇ persists in *TcPI-PLC1*-KO epimastigotes. Values are expressed as means \pm SD (n > 3) * $P \le 0.01$; ** $P \le 0.01$; ** $P \le 0.01$ by Student's t test.

effect on trypomastigote infection of host cells (Fig. 6H) and amastigote replication (Fig. 6I).

We then investigated whether synthesis of inositol phosphates was affected in *TcPl-PLC1*-KO epimastigotes (Fig. 6J and K). Inositol phosphates were extracted from *TcPl-PLC1*-KO cells and control cells transfected with scrambled sgRNA using titanium beads, following the previously described method (38). The extracted inositol polyphosphates were then analyzed by capillary electrophoresis-electrospray ionization-mass spectrometry (CE-ESI-MS) (39, 40), using 13 C-labeled internal references (41). Fig. 6K shows the detection of 5-IP $_7$ in epimastigote extracts of *T. cruzi*. Interestingly, an IP $_7$ not previously identified (pyrophosphorylated in C-1 or C-3, as they are enantiomers and thus indistinguishable by CE-MS) in *T. cruzi* was detected (Fig. 6J). Fig. 6K shows that the levels of IP $_6$, 1/3-IP $_7$, and 5-IP $_7$ were not decreased in the *TcPI-PLC1*-KO cells; instead, levels of IP $_6$ and 1/3-IP $_7$ were slightly increased, while levels of IP $_3$ -2 did decrease. In conclusion, TcPI-PLC1 does not appear relevant for the synthesis of inositol polyphosphates in *T. cruzi* epimastigotes, although it is important for IP $_3$ -2 formation.

Having seen that a PLC-independent pathway is operative in *T. cruzi*, we devised a set of experiments aimed at defining which alternative substrates could feed the IP pool. To investigate whether 3-IP₁ produced from glucose 6-phosphate by the inositol 3-phosphate synthase could also be used *in vivo* as a substrate of ITPK1 to generate inositol polyphosphates, we grew wild-type and *TcPI-PLC1*-KO *T. cruzi* epimastigotes with 1-¹³C-D-glucose and measured the formation of inositol phosphates. These KO cells were able to synthesize IP₆₋₈ from glucose, as detected by LC-MS (19) of epimastigote extracts (Fig. 7), demonstrating the presence of the alternative pathway for the synthesis of IPs from G6P. Interestingly, while labeling of IP₂ and IP₃ decreased significantly in the *TcPI-PLC1*-KO mutants, no significant differences were detected in the labeling of IP₆₋₈, suggesting that the lipid-dependent pathway is important for the formation of IP₃ but not for the formation of IP₆₋₈ under these conditions (Fig. 7).

$\it TclSC1$ knockout cells produce less $\it IP_6$ and are unable to infect tissue culture cells

To investigate whether the expression of TcISC1 was important to generate 1-IP₁ from inositol phosphoceramide (IPC) as a source of inositol polyphosphates, we utilized a T7RNAP/Cas9 strategy to generate KO mutants of this gene (Fig. 8A). The KO was validated by PCR (Fig. 8B) and Southern blot analysis (Fig. 8C; Fig. S5C). Proliferation of TcISC1-KO epimastigotes was significantly affected (Fig. 8D) but metacyclogenesis was not (Fig. 8E). To investigate the importance of TcISC1 to produce IP₆, we extracted IPs from large amounts of cells and tested extracts by 35% polyacrylamide gel electrophoresis. A band that runs like the IP₆ standard and that disappears after treatment of the extracts with phytase was detected. The densitometric analysis revealed that the band was significantly decreased in TcISC1-KO cells, revealing that TcISC1 participates in the synthesis of IP₆ through the conversion of IPC into 1-IP₁ (Fig. 8F and G). Several attempts (n = 3) to infect tissue culture cells with TcISC1-KO metacyclic forms failed and did not result in recovery of cell-derived trypomastigotes, suggesting that TcISC1 is important for infectivity.

C-terminal tagging of TcISC1 (Fig. 9A) was validated by Western blot analysis (Fig. 9B) and PCR (Fig. 9C), and the enzyme was found to co-localize with the endoplasmic

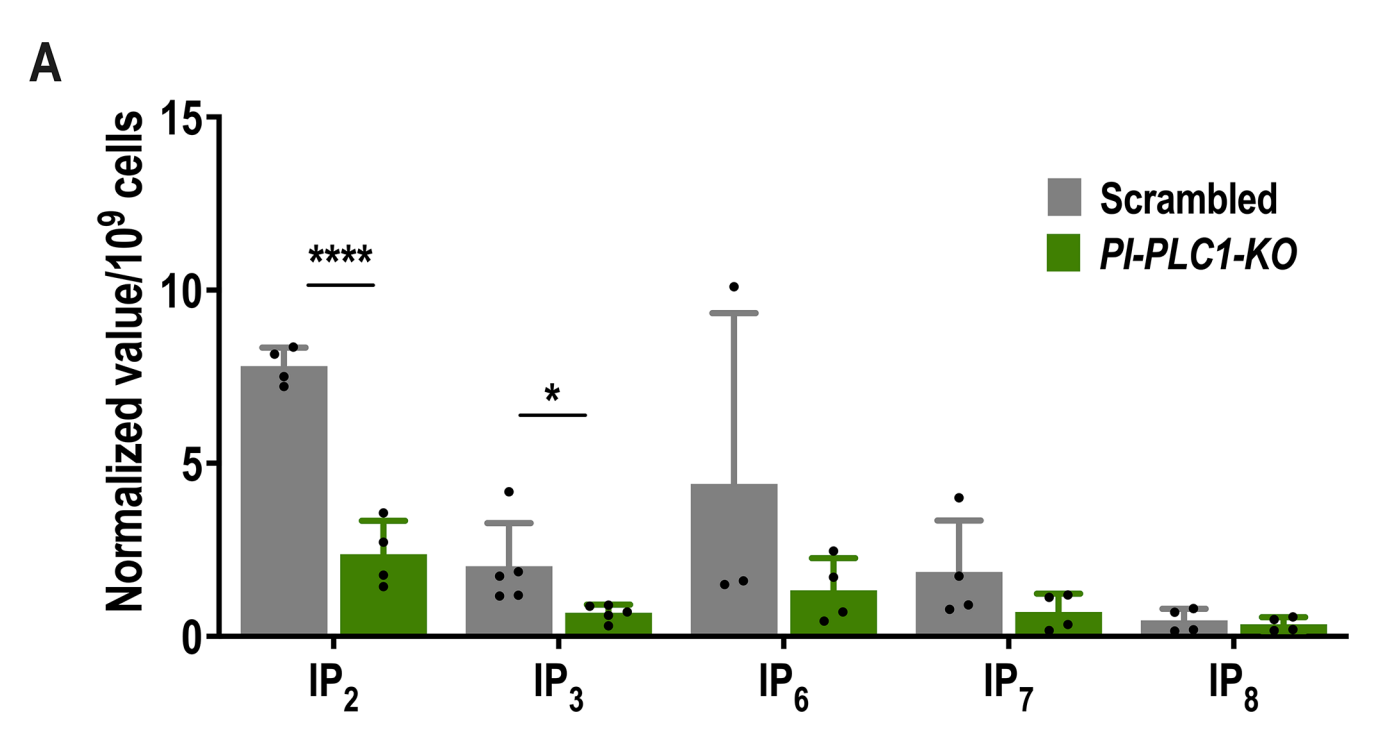


FIG 7 Glucose labeling for inositol phosphate detection. (A) Metabolic labeling was performed by cultivating *T. cruzi* epimastigotes at an initial density of 2 \times 10⁶ cells/mL in low-glucose LIT medium (no added glucose) for 48 hours. After this period, the parasites were harvested by centrifugation and resuspended in fresh LIT medium containing either 10 mM ¹³C-labeled D-glucose or 10 mM unlabeled D-glucose. The cultures were incubated for an additional 48 hours. Subsequently, the cells were harvested by centrifugation for inositol phosphate extraction and LC-MS analysis. Values are expressed as means \pm SD (n > 3) * $P \le 0.005$; ***** $P \le 0.0001$ by Student's t test.

reticulum marker BiP (Fig. 9D) and the mitochondrial marker MitoTracker (Fig. 9E). Overexpression of *TcISC1* (Fig. 9F) did not affect epimastigote growth (Fig. 9G) and confirmed the dual localization in the ER (Fig. 9H) and mitochondria (Fig. 9I).

DISCUSSION

The main finding of this work is that in *T. cruzi*, the pathway for the formation of inositol phosphates using the TcPI-PLC1 is mainly involved in IP₃ formation, which is crucial for Ca²⁺ signaling, trypomastigote invasion of host cells, and amastigote replication. Meanwhile, the PI-PLC1-independent, or cytosolic, pathway is involved in the formation of inositol polyphosphates from endogenous sources via glucose 6-phosphate or inositolphosphoceramide, leading to inositol monophosphate production. This pathway is essential for parasite survival.

The hypothetical protein TcYC6_0083580 was identified as an inositol tetrakisphosphate kinase 1 (ITPK1). We used a bioinformatic toolset to establish the evolutionary relationship and structural conservation of TcITPK1. Initial results of multiple alignment of protein sequences demonstrated that TcITPK1 shares two out of three highly conserved residues and three out of four less conserved residues required for inositol phosphate- and ATP-binding of the protein.

The phylogenetic study demonstrated that ITPK1 is present in kinetoplastids and other higher-order eukaryotes and that most critical residues are conserved. This finding was also noted in a recent review on the inositol phosphate pathway in higher-order eukaryotes (42). *T. cruzi* is found in the Discoba supergroup of eukaryotes, whereas *Homo sapiens* is a member of the Opisthokonta supergroup (43). While both organisms are in different eukaryotic supergroups, the evidence suggests that their last eukaryotic common ancestor had this lipid-independent, cytosolic pathway to synthesize inositol polyphosphates from glucose 6-phosphate without the need for PLC. The absence of this

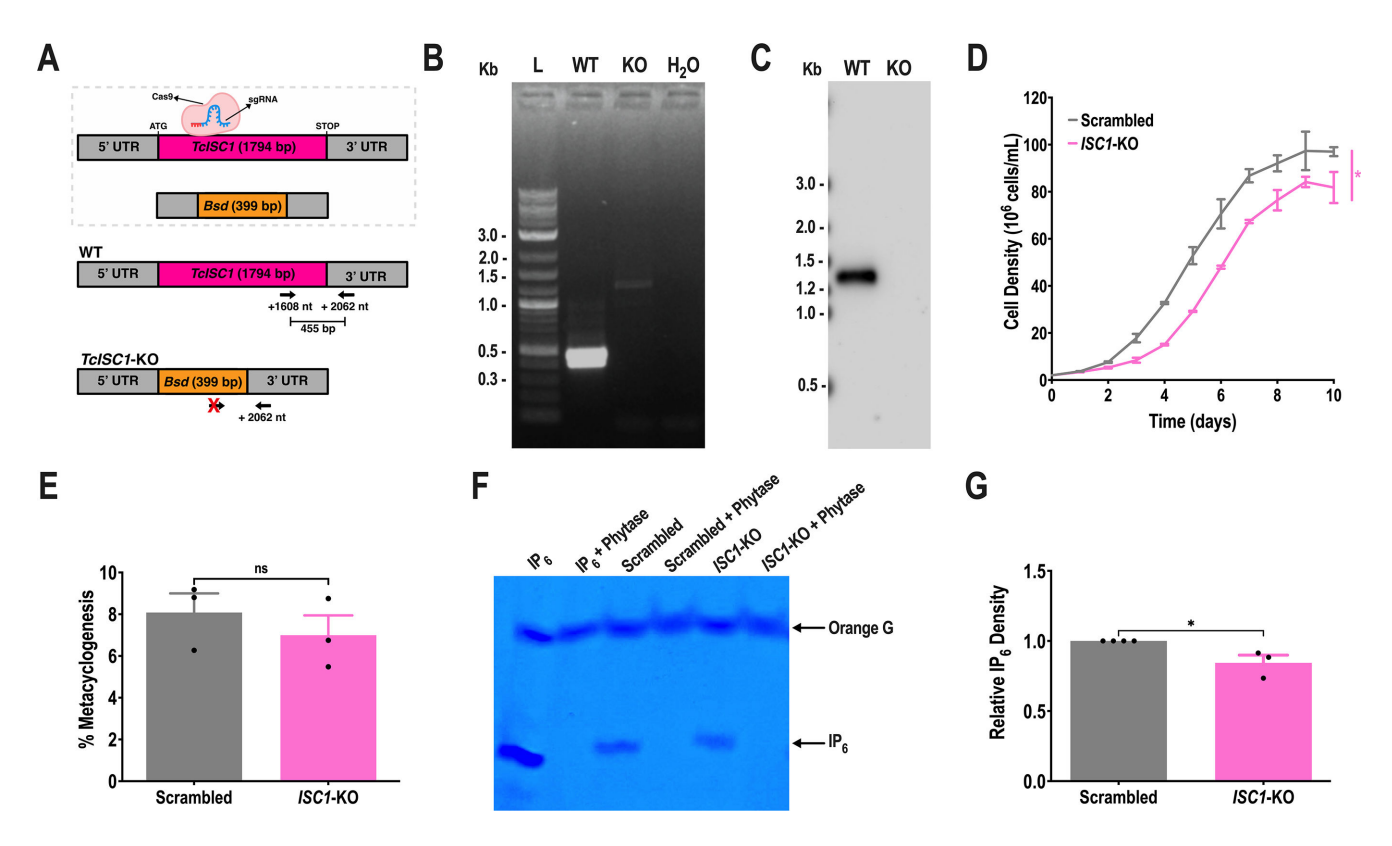


FIG 8 Knockout of *TcISC1*. (A) Schematic representation of the strategy used to generate a *TcISC1*-KO mutant by homologous recombination and primers (arrows) used to verify gene replacement by PCR. The intact locus generates a PCR product of 455 bp, while the disrupted locus does not generate a fragment. (B) PCR analysis showing that *TcISC1* was ablated at its genomic locus and replaced in genomic DNA of the KO cell line. Lanes: L, 1 kb plus ladder; WT, wild-type; KO, *TcISC1*-KO; H₂O, PCR-negative control. (C) Southern blot analysis of wild-type and *TcISC1*-KO (KO) gDNA digested with the Pvull restriction enzyme. The blot was hybridized with a biotin-labeled probe corresponding to 435 bp of *TcISC1* (nt +694 to +1,128), revealing a 1,295-bp band only for Pvull-digested gDNA from WT cells. (D) Growth of control (scrambled) and *TcISC1*-KO (*ISC1*-KO) epimastigotes in the LIT medium. Values are expressed as means \pm SD (n = 3) * $P \le 0.05$ by Student's t = 1.00 test. (E) Percentage of metacyclic trypomastigotes in epimastigote cultures after incubation in the TAU 3AAG medium. Values are expressed as means $t \le 1.00$ power treated with phytase (0.1 mg/mL, pH 5.0, at 37°C for 1 hours) to confirm that the bands correspond to IP₆. (G) Densitometry of toluidine-stained IP₆ from scrambled and *TcISC1*-KO. Values are expressed as means $t \le 1.00$ 0 pc 50.00 by Student's t = 1.000 pc 50.00 pc

pathway in apicomplexans appears as a recent acquisition of that clade and does not reflect the overall evolution of this pathway.

Immunofluorescent assays of CRISPR/Cas9 endogenously tagged *TcITPK1* demonstrated that TcITPK1 localizes to the cytosol. The failed attempts to generate a CRISPR/Cas9-mediated *TcITPK1* knockout and knockdown suggest that *TcITPK1* may be an essential gene in *T. cruzi* epimastigotes and that the lipid-independent pathway plays an important role in parasite survival. In this regard, the INO1 has been shown to be essential for their survival (44), while we found that *TcISC1*-KO cells are unable to infect mammalian cells.

TcPI-PLC1 is lipid-modified at its N-terminus and plays an essential role in cell signaling (45–48). We were able to knockout *TcPI-PLC1* in epimastigotes despite previous unsuccessful attempts that suggested its essentiality (47). However, the proliferation of *TcPI-PLC1*-KO epimastigotes was affected, while trypomastigote host cell invasion and intracellular amastigote replication were significantly reduced. The effect on amastigote replication could be related to the inhibition of trypomastigote to amastigote differentiation observed when *TcPI-PLC1* expression was downregulated by antisense oligonucleotides (47).

TcPI-PLC1 genetic knockout in *T. cruzi* epimastigotes does not stop the formation of higher-order inositol phosphates, demonstrating the existence of an alternative

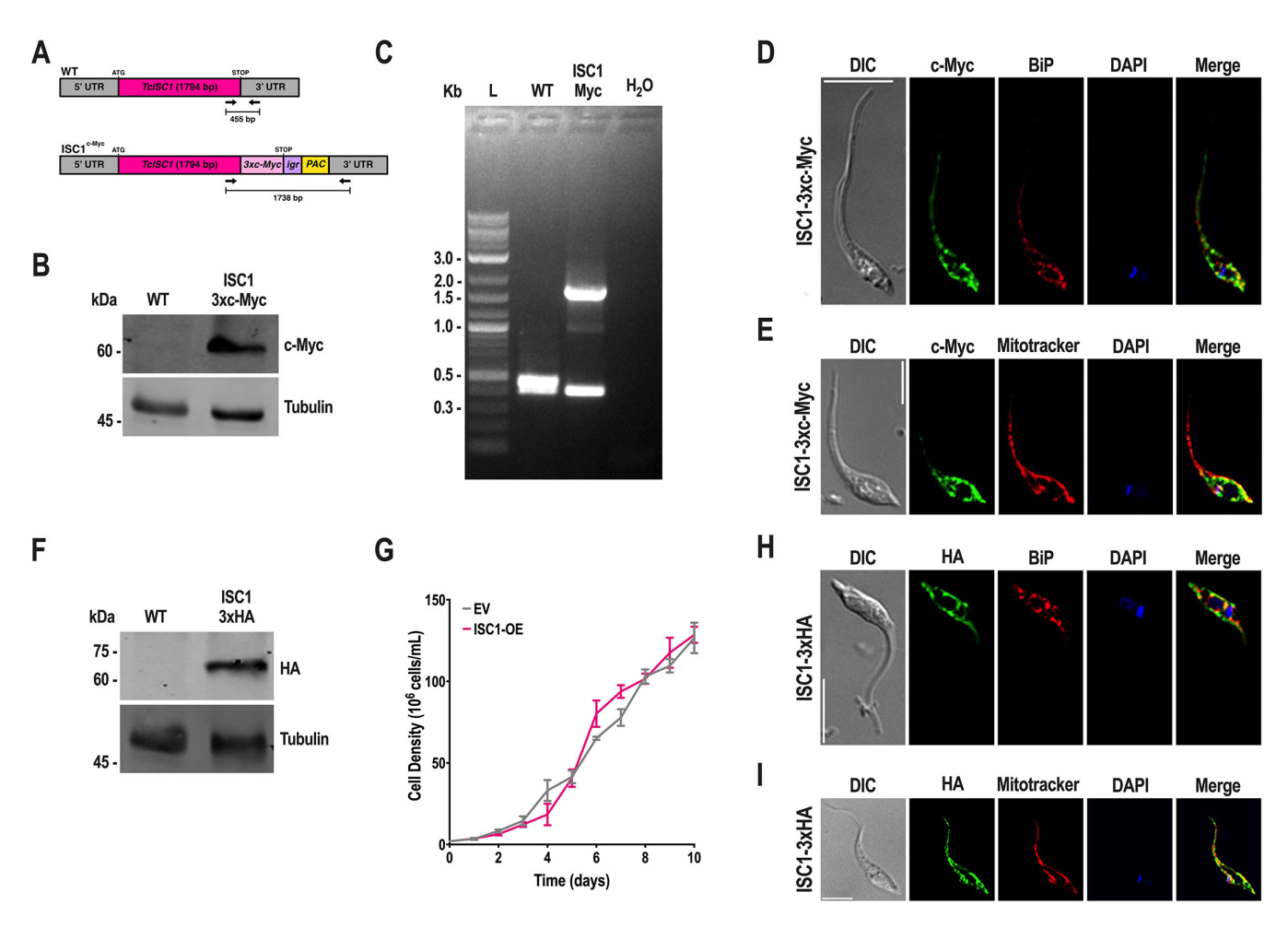


FIG 9 CRISPR/Cas9 endogenous C-terminal tagging and overexpression of *TcISC1*. (A) Schematic representation of the wild-type and endogenous tagged *TcISC1* gene. Epimastigotes were endogenously tagged with a 3×c-Myc tag using CRISPR/Cas9 genome editing. (B) PCR analysis for validation of *TcISC1* tagging showing expected bands for control cell lines (WT, predicted size, 455 bp) and *TcISC1*-3×c-Myc cell line (ISC1 Myc, predicted size, 1,738 bp). (C) Western blot analysis of wild-type and TcISC1-3×c-Myc epimastigotes using monoclonal antibodies against c-Myc tag. The predicted protein molecular mass for TcISC1-3×c-Myc was 72 kDa. Molecular markers are on the left. Tubulin was used as a loading control. (D) Localization of endogenously tagged TcISC1-3×c-Myc in epimastigotes using anti-c-Myc antibodies. DIC, differential interference contrast. *c*-Myc (green), TcISC1-3×c-Myc. BiP (red), endoplasmic reticulum marker. The merge image shows that TcISC1-3×c-Myc in epimastigotes using anti-c-Myc antibodies. DIC, differential interference contrast. *c*-Myc (green), TcISC1-3×c-Myc. Mitotracker (red), mitochondrial marker. The merge image shows that TcISC1-3×c-Myc (green) colocalizes with Mitotracker (red); PCC = 0.60. Scale bar = 5 μm. (F) Western blot analysis of wild-type and TcISC1-3×HA epimastigotes using monoclonal antibodies against the HA tag. The predicted protein molecular mass for TcISC1-3×HA (ISC1-OE) epimastigotes in the LIT medium. (H) Localization of TcISC1-3×HA in epimastigotes using anti-HA antibodies. DIC, differential interference contrast. HA (green), TcISC1-3×HA. BiP (red), endoplasmic reticulum marker. The merge image shows that TcISC1-3×HA (green) colocalizes with BiP (red); PCC = 0.67. Scale bar = 5 μm. (I) Localization of TcISC1-3×HA in epimastigotes using anti-HA antibodies. DIC, differential interference contrast. HA (green), TcISC1-3×HA. Mitotracker (red), mitochondrial marker. The merge image shows that TcISC1-3×HA (green) colocalizes with Mitotracker (red); PCC = 0.67. Scale bar = 5 μm.

synthesis pathway. *S. cerevisiae* genetic screens were employed to determine its capabilities to phosphorylate inositol monophosphate and other inositol phosphate species. SAX-HPLC experiments demonstrated that complementation of *S. cerevisiae plc1* Δ with *TcITPK1* rescues the synthesis of IP₆. This result is also in agreement with previous results on HsITPK1 (22) and the positive control. There are three highly conserved residues that are important for IP- and ATP-binding—H167, K199, and R212—in HsITPK1. TcITPK1 only shares two of these conserved residues, and therefore this may explain the differences in the overall rescue of IP₆ synthesis. However, attempts to knockout the lipid-independent inositol phosphate synthesis pathway in *TcITPK1*-KO experiments resulted in the death of

parasite cultures, so this lesser rescue was unexpected. In contrast, *S. cerevisiae* growth assays demonstrate TcITPK1 was able to rescue the growth of *S. cerevisiae* $plc1\Delta$. This impact may be due to the formation of inositol phosphate species, an important molecule to a variety of yeast cellular processes including regulation of major glycolytic transcription factor GCR1, pseudohyphal growth, and ATP concentration (49, 50). The *S. cerevisiae* phosphoinositide-specific phospholipase C gene (*PLC1*) is a homolog to *TcPl-PLC1* and other delta class PLC enzymes, and the knockdown of *plc* causes organisms to over accumulate PIP₂ and fail to synthesize inositol phosphate (22). The lagging growth phenotype in *myo*-inositol-deficient media further demonstrates the importance of inositol phosphate species synthesis as these samples took longer to reach the stationary phase. However, complementation with either eukaryotic ITPK1 enzymes—be it TcITPK1 or HsITPK1—allowed for the rescue of this growth deficiency.

As it has been proposed before (22), the occurrence of two independent pathways for inositol phosphate metabolism, one associated with the formation of the Ca²⁺ signaling agent IP3 and the other associated with the production of inositol pyrophosphates, suggests different compartmentalization. In this regard, pools of independently cycling inositol phosphates have been reported in human cells (51). This is supported by results in T. brucei, where uptake of [3H]inositol did not result in detection of IP6, while IP6 was easily detected by PAGE analyses suggesting an endogenous origin (18). In addition, it has been demonstrated that in T. brucei, the formation of phosphoinositides and IP3 depends on exogenous inositol uptake, while synthesis of GPI anchors requires endogenous synthesis of inositol. As we described in Fig. 1, endogenous synthesis of inositol phosphates could occur by the conversion of G6P into 3-IP₁ catalyzed by INO1, or by the conversion of IPC into 1-IP_{1,} catalyzed by ISC1. In this work, we demonstrate that TcITPK1 can use both 1-IP1 generated from IPC in yeast or T. cruzi and 3-IP1 generated from G6P in *T. cruzi*. The production of 1-IP₁ from IPC could be important in T. cruzi because IPC is abundant in characteristic GPI anchors of T. cruzi, like those in the trans-sialidase of trypomastigotes (52), and the surface protein Ssp4 of amastigotes (53). IPC is also present in the anchor of mucins of metacyclic trypomastigotes (54). A free glycoinositol phospholipid (GIPL) originally named lipopeptide phosphoglycan (LPPG) is the major glycoconjugate of *T. cruzi* epimastigotes and also has IPC (55).

Another potential source of IPC is by salvage of lipids from the host cells and remodeling in the mammalian stages, as occurs in *Leishmania* (10, 11). Knockout of *L. mexicana* IPC synthase affects the synthesis of IP₂ and IP₆ (56), which agrees with the present study's findings. Disruption of *T. cruzi* IPC synthase has been shown to affect metacyclogenesis, intracellular amastigote proliferation, and differentiation of amastigotes into tissue culture-derived trypomastigotes, preventing the establishment of infection *in vivo* in immune-deficient mice (57). In agreement with that report, we found that *TcISC1*-KO parasites were unable to infect host cells. This effect could be related to the reported hypersensitivity to acidic stress of knockout mutants of *Isc1* in *Cryptococcus neoformans* (58) and *Leishmania major* (59), which prevents their proliferation in the macrophage phagolysosomes. In this regard, *T. cruzi* also occupies an acidic phagolysosome upon entry into the host cells (60), which is needed to differentiate the infective trypomastigotes into replicating amastigotes. As occurs with *S. cerevisiae* ISC1 (61, 62), TcISC1 has a dual localization in the ER and mitochondria.

In summary, while the TcPLC1 pathway is important for generating IP₃, which is needed for Ca²⁺ signaling, the TcPLC1-independent, or cytosolic, pathway is involved in the generation of inositol polyphosphates. The essential role of this pathway in the infection of host cells by *T. cruzi* suggests that the enzymes involved could serve as potential drug targets, indicating the possibility of developing inhibitors.

MATERIALS AND METHODS

Clustal omega analysis

Ten homologous ITPK1 amino acid sequences of interest were identified from *Lokiarchaeum candidatus, Entamoeba histolytica, Oryza sativa, Zea mays, Monosiga brevicollis, Dictyostelium discoideum, Danio rerio, Gallus gallus, Homo sapiens,* and *Mus musculus* from a previous publication (22). A potential TcITPK1 homolog was identified in TriTrypDB as TcYC6_0083580 (GenBank KAF8297109.1) (63). A FASTA file containing all eleven homologous amino acid sequences was uploaded to Clustal Omega Multiple Sequence Alignment, and default multiple sequence alignment parameters were used (64).

Constructing an ITPK1 phylogenetic tree

The initial amino acid sequence for *T. cruzi* inositol tetrakisphosphate 1-kinase (TcITPK1) was obtained from TriTrypDB. TriTrypDB and OrthoMCL search analyses were performed using the full-length protein sequence of the *T. cruzi* ITPK1 protein (TcYC6_0083580) and orthology group number (OG6_147480) (63, 65). In addition, five selected ITPK1 predicted orthologs were added to the compilation of identified orthologs for a total of 27 unique sequences. The bootstrap consensus tree inferred from 1,000 replicates was taken to represent the evolutionary history of the taxa analyzed. Branches corresponding to partitions reproduced in less than 50% bootstrap replicates are collapsed. The percentage of replicate trees in which the associated taxa clustered together in the bootstrap test (1,000 replicates) were shown next to the branches. The evolutionary distances were computed using the JTT matrix-based method and are expressed in the units of the number of amino acid substitutions per site. The rate variation among sites was modeled with a gamma distribution (shape parameter = 4). All ambiguous positions were removed for each sequence pair (pairwise deletion option). There was a total of 773 positions in the final data set. Evolutionary analyses were conducted in MEGA11.

AlphaFold-2.1.1 prediction and modeling of TcITPK1 and HsITPK1

AlphaFold Version 2.1.1 was installed on the Sapelo2 cluster by the Georgia Advanced Computer Center (GACRC) of the University of Georgia using EasyBuild following the steps in the dockerfile available at (25). The run_alphafold.sh bash script was obtained from https://github.com/kalininalab/alphafold_non_docker, and related documentation is available at that URL. The run_alphafold.sh bash script was edited to run the FASTA file containing the amino acid sequence for either TcITPK1 or HsITPK1 using the monomer_casp14 modeling parameters.

Protein structural comparison analysis

Pairwise structure alignment is a tool on the RCSB Protein Data Bank website that allows for the comparison of two or more protein structures (28–34). As a built-in control for AlphaFold-2.1.1 prediction accuracy, the best model for HsITPK1 predicted by the AlphaFold-2.1.1 Monomer_Casp14 algorithm was compared to the X-ray diffraction-resolved HsITPK1 (2ODT) structure using the jFATCAT (flexible) parameter (35). Pairwise structural alignment outputs a table describing the RMSD, TM-Score, Score, SI%, SS%, and overall length of the structures selected/uploaded for superposition. Structural comparison was repeated at FATCAT using the FATCAT (flexible) to find the significance of structural comparisons (33). This protein structural comparison analysis pipeline was repeated for the best AlphaFold-2.1.1-predicted model for TcITPK1 and X-ray diffraction-resolved HsITPK1 (2ODT) structure.

Chemical and reagents

Platinum Taq DNA Polymerase High-Fidelity, BCA protein assay kit, Alexa-conjugated secondary antibodies, MitoTracker deep red FM, Chemiluminescent Nucleic Acid Detection Module, and BioPrime DNA Labeling System kit were obtained from Thermo

Fisher Scientific (Waltham, MA). The BLUelf prestained protein ladder was obtained from FroggaBio (Wheatfield, NY). The anti-c-Myc monoclonal antibody (clone 9E10) was from Santa Cruz Biotechnology (Dallas, TX). Puromycin was from Acros Organics (Fair Lawn, NJ). Blasticidin S HCl was purchased from Life Technologies (Grand Island, NY). Wizard plus SV miniprep Purification System, Wizard SV Gel and PCR Clean-up System, GoTag DNA polymerase, and T4 DNA ligase were from Promega (Madison, WI). Antarctic phosphatase, restriction enzymes, and Q5 High-Fidelity DNA Polymerase were from New England Biolabs (Ipswich, MA). Fluoromount-G was from SouthernBiotech (Birmingham, AL). The primers were purchased from Integrated DNA Technologies. The Nitrocellulose Membranes were from Bio-Rad (Hercules, CA). G418 sulfate was from KSE Scientific (Durham, NC). The anti-HA mouse monoclonal antibody was from BioLegend (San Diego, CA). Anti-tubulin monoclonal antibody, anti-glutathione-S-transferase rabbit polyclonal antibody, mammalian cell protease inhibitor mixture (Sigma P8340), other protease inhibitors, Benzonase Nuclease, and all other reagents of analytical grade were from Sigma (St. Louis, MO). The rabbit polyclonal antibody against TbBiP (66) was provided by Dr. Jay Bangs (University at Buffalo, NY).

Culture methods

 $T.\ cruzi$ (Y strain) epimastigotes were maintained at 28°C in the LIT medium (67), supplemented with 10% newborn calf serum (NCS), penicillin (100 U mL⁻¹), and streptomycin (100 µg mL⁻¹). Mutant cell lines were maintained in the medium containing 250 µg/mL G418, 10 µg/mL blasticidin, or 5 µg/mL puromycin. The growth rate of epimastigotes was determined by counting cells every 24 hours using a Coulter Counter (Beckman Coulter). Tissue culture cell-derived trypomastigotes were obtained from Vero cells infected with metacyclic trypomastigotes as described below. *T. cruzi* trypomastigote forms were collected from the culture medium of infected host cells, using a modification of the method of Schmatz and Murray (68), as described previously (69). Vero cells were grown in RPMI supplemented with 10% fetal bovine serum (FBS) and maintained at 37°C with 5% CO₂.

TcITPK1 and TcISC1 overexpression

TcITPK1 and *TcISC1* open reading frames (ORF) (1,260 and 1,794 nt, respectively) were PCR-amplified using *T. cruzi* Y strain gDNA as the template (primers 31, 32, 33, and 34; Table S1) and cloned into the pTREX-n/3×HA vector by restriction sites Xbal/Xhol. Gene cloning was confirmed by PCR and sequencing, and constructs were subsequently used to transfect *T. cruzi* epimastigotes. *TcITPK1* and *TcISC1* overexpression was confirmed by Western blot analysis using anti-HA antibodies.

CRISPR/Cas9 endogenous C-terminal tagging.

Targeted sgRNAs for endogenous C-terminal tagging (3'-end) were amplified in a one-step PCR using a forward oligonucleotide primer (Table S1, primer 10 or 42), universal reverse primer (Table S1, primer 45), and pUC_sgRNA plasmid as a template. This PCR step was followed by PCR purification. The specific sgRNA was cloned into the Cas9/pTREX-n vector (Addgene plasmid #68708) (36), and alignment was verified by Sanger sequencing (Table S1, primer 46). Donor DNA was synthesized for endogenous C-terminal tagging in a one-step PCR using the pMOTag23M DNA vector as the DNA template and long ultramers (Table S1, primers 11–12 and 43–44). After visualization of donor DNA on an agarose gel, DNA was purified by phenol/chloroform/isoamyl alcohol (25:24:1) extraction and quantified by NanoDrop spectrophotometry. Epimastigotes were co-transfected with sgRNA/Cas9/pTREX-n and DNA donor and then cultured for 5 weeks with G418 and puromycin for selection of double-resistant parasites. Endogenous gene tagging was verified by PCR from gDNA using specific primer sets (Table S1, primers 13–14 and 38–39) and by Western blot analysis.

Knockout of TcPI-PLC1

Chimera single-guide RNA (sgRNA) sequences to target the TcPI-PLC1 gene (TcYC6_0042910; AB022677.1) were PCR-amplified (Table S1, primers 1 and 47) from plasmid pUC_sgRNA, as previously described (36). Selection of the protospacer was performed using EuPaGDT (Eukaryotic Pathogen CRISPR guide RNA Design Tool, http:// grna.cteqd.uga.edu/). The protospacer sequence was included in the forward primer, while using a common reverse primer for sgRNA amplification. The sgRNA orientation was verified by PCR using the specific TcPI-PLC1-sqRNA forward primer and the HX1 reverse primer (Table S1, primers 1 and 46) (36). Positive clones that generate a 190bp PCR fragment were also sequenced. A scrambled sgRNA (scrambled-sgRNA/Cas9/ pTREX-n) was used as control. A DNA donor cassette designed to promote homologous directed repair and replacement of TcPI-PLC1 ORF was obtained by PCR using a set of long primers (ultramers) containing 120 nucleotides, from which 100 nucleotides correspond to the first 100 nt (forward ultramer) and the last 100 nt (reverse ultramer) of TcPI-PLC1 ORF, and 20 nt annealing on the blasticidin gene (Table S1, primers 2 and 3). The TcPI-PLC1-sqRNA/pTREX-p construct and linear blasticidin cassette were used to transfect epimastigotes. After 5 weeks of selection with 250 µg/mL G418 and 10 µg/mL blasticidin, TcPI-PLC1 gene replacement was verified by PCR using primers 8 and 9 (Table S1).

Knockout of TcITPK1

The knockout strategy using the T7RNAP/Cas9 was designed and performed as previously described (37). Chimera single-guide RNA (sgRNA) sequences to target the TcITPK1 gene (TryTripDB identifier [ID] TcYC6_0083580) were PCR-amplified (Table S1, primers 15 and 16). Selection of the protospacer was performed using EuPaGDT (Eukaryotic Pathogen CRISPR guide RNA Design Tool, http://grna.ctegd.uga.edu/). The protospacer sequence and the T7 polymerase-binding site were included in the forward primer, while using a common reverse primer for sgRNA amplification. A DNA donor cassette designed to promote homologous directed repair and replacement of TcITPK1 ORF was obtained by PCR using a set of primers (Table S1, primers 17 and 18). The forward primer contains a 40-nt 5'UTR-containing homologous region (HR) plus 20 nucleotides of the plasmid backbone including the start codon (5'-GCCGCGGGAATTC GATTATG-3'). The reverse primers consist of 37 nucleotides of the 3'UTR-containing HR followed by 23 nucleotides of the plasmid backbone and the four last nucleotides of the antibiotic resistance genes, including the stop codon (5'-CGCGAATTCACTAGTG ATTTCAC-3'). To amplify the donor DNA cassettes, the plasmids pBSD or pPAC were used as templates. We co-transfected T. cruzi T7RNAP/Cas9 epimastigotes with the sgRNA template and one (puromycin) or two (puromycin and blasticidin) donor DNAs. Transfected parasites were cultured for 4 weeks in the presence of G418 and puromycin, or G418, puromycin, and blasticidin for selection of single- or double-KO parasites, respectively. Gene disruption was verified using gDNA from mutant parasites by PCR using primers 19 and 20 (Table S1).

Knockout of TcISC1

The knockout strategy using the T7RNAP/Cas9 was designed and performed as previously described (37). Chimera single-guide RNA (sgRNA) sequences to target the *TcISC1* gene (TcYC6_0066130; KAF8297109.1) were PCR-amplified (Table S1, primers 15 and 35). Selection of the protospacer was performed using EuPaGDT (Eukaryotic Pathogen CRISPR guide RNA Design Tool, http://grna.ctegd.uga.edu/). The protospacer sequence and the T7 polymerase-binding site were included in the forward primer, while using a common reverse primer for sgRNA amplification. A DNA donor cassette designed to promote homologous directed repair and replacement of *TcISC1* ORF was obtained by PCR using a set of primers (Table S1, primers 36 and 37). The forward primer contains a 40-nt 5'UTR-containing homologous region (HR) plus 20 nucleotides

of the plasmid backbone including the start codon (5'-GCCGCGGGAATTCGATTATG-3'). The reverse primers consist of 37 nucleotides of the 3'UTR-containing HR followed by 23 nucleotides of the plasmid backbone and the four last nucleotides of the antibiotic resistance genes, including the stop codon (5'-CGCGAATTCACTAGTGATTTCAC-3'). To amplify the donor DNA cassettes, the plasmids pBSD or pPAC were used as templates. We co-transfected *T. cruzi* T7RNAP/Cas9 epimastigotes with the sgRNA template and one (puromycin) or two (puromycin and blasticidin) donor DNAs. Transfected parasites were cultured for 4 weeks in the presence of G418 and puromycin, or G418, puromycin, and blasticidin, for selection of single- or double-KO parasites, respectively. Gene disruption was verified using gDNA from mutant parasites by PCR using primers 38 and 39 (Table S1).

Cell transfection

Transfections were performed as previously described (70). Briefly, *T. cruzi* Y strain epimastigotes (4 \times 10 7 cells) were washed with phosphate-buffered saline (PBS), pH 7.4, at room temperature (RT) and transfected in ice-cold CytoMix (120 mM KCl, 0.15 mM CaCl $_2$, 10 mM K $_2$ HPO $_4$, 25 mM HEPES, 2 mM EDTA, 5 mM MgCl $_2$, pH 7.6) containing 25 μg of each plasmid construct in 4-mm electroporation cuvettes with three pulses (1,500 V, 25 μF) delivered by a Gene Pulser Xcell Electroporation System (Bio-Rad). Stable cell lines were established and maintained under drug selection with appropriate antibiotic(s) (250 $\mu g/mL$ G418, 10 $\mu g/mL$ blasticidin, and/or 5 $\mu g/mL$ puromycin). Transfectant epimastigotes were cultured in the LIT medium supplemented with 20% heat-inactivated NCS until stable cell lines were obtained. Parasite clones were obtained by limiting dilution.

Western blot analyses

Transfected T. cruzi epimastigotes were harvested separately. Parasites were washed twice in PBS and resuspended in radioimmunoprecipitation assay buffer (RIPA: 150 mM NaCl, 20 mM Tris-HCl [pH 7.5], 1 mM EDTA, 1% SDS, and 0.1% Triton X-100) plus a mammalian cell protease inhibitor mixture (diluted 1:250), 1 mM phenylmethylsulfonyl fluoride, 2.5 mM tosyl phenylalanyl chloromethyl ketone (TPCK), 100 μM N-(trans-epoxysuccinyl)-L-leucine 4-guanidinobutylamide (E64), and benzonase nuclease (25 U/mL of culture). The cells were incubated for 1 hour on ice, and the protein concentration was determined by the BCA protein assay. Thirty micrograms of protein from each cell lysate was mixed with 4× Laemmli sample buffer (125 mM Tris-HCl, pH 7, 10% [wt/vol] β-mercaptoethanol, 20% [vol/vol] glycerol, 4.0% [wt/vo]l SDS, and 4.0% [wt/ vol] bromophenol blue) before application to 10% SDS-polyacrylamide gels. Separated proteins were transferred onto nitrocellulose membranes with a Bio-Rad Trans-blot apparatus. Membranes were blocked with 5% nonfat dried skim milk in PBS-T (PBS containing 0.1% [vol/vol] Tween 20) overnight at 4°C. Next, membranes were incubated for 1 hour, at RT, with a primary antibody, i.e., monoclonal anti-HA (1:1,000), monoclonal anti-c-Myc-tag (1:100), or monoclonal anti-tubulin (1:20,000). After three washes with PBST, blots were incubated with the appropriate secondary antibody for 1 hour, at RT, in the dark, i.e., IRDye 680RD-conjugated goat anti-rabbit IgG (1:10,000) or IRDye 800CW-conjugated goat anti-mouse IgG (1:10,000). Blots were washed three times with PBST, and Western blot images were obtained and processed with the Odyssey infrared imaging system (LI-COR Biosciences).

Immunofluorescence assays

T. cruzi epimastigotes were washed with PBS and fixed with 4% paraformaldehyde in PBS for 1 hour, at RT. To determine mitochondrial localization of ISC 1 proteins, epimastigotes were incubated with 100 nM MitoTracker deep red FM for 30 minutes at 28°C in the culture medium before the fixing procedure. Cells were allowed to adhere to poly-L-lysine-coated coverslips and then permeabilized for 5 minutes with 0.1% Triton

X-100. Permeabilized cells were blocked with PBS containing 3% BSA, 1% fish gelatin, 50 mM NH₄Cl, and 5% goat serum overnight at 4°C. Then, cells were incubated with a primary antibody (monoclonal anti-HA [1:50] or monoclonal anti-c-Myc-tag [1:10]), diluted in 1% BSA in PBS (pH 8.0) for 1 hour, at RT. Rabbit anti-TbBiP antibodies were used at a dilution of 1:500. Cells were washed three times with 1% BSA in PBS (pH 8.0) and then incubated for 1 hour, at RT, in the dark with Alexa Fluor 488- or Alexa Fluor 546-conjugated goat anti-mouse secondary antibodies (1:1000).

Immunofluorescence of yeast was performed as described (71), with some modifications. Briefly, mid- to late-log phase yeast cells were centrifuged at $700 \times g$ for 5 minutes and fixed with 4% paraformaldehyde in SC-URA on a shaker (200 rpm) at 30°C for 1 hour. Cells were collected by centrifugation, washed once with 1 mL of the fresh medium, and incubated with DET (100 mM DTT, 20 mM EDTA, 20 mM Tris-HCl, pH 8.0) at RT for 5 minutes. After collecting the cells by centrifugation, the cell pellet was suspended in 1 mL of 0.9 M sorbitol/PBS (pH 7.4), 20 mg/mL zymolyase was added to make a final concentration of 100 μ g/mL, and then incubated on a shaker (200 rpm) for 30–60 minutes at 37°C until cell walls were digested. Spheroplasts were washed gently with 0.9 M sorbitol/PBS, allowed to adhere to poly-L-lysine-coated coverslips, and permeabilized with 1% Triton X-100/0.9 M sorbitol/PBS (pH 7.4) for 10 minutes at RT. After blocking with PEM (100 mM PIPES [pH 7.0], 1 mM EGTA, 0.1 mM MgSO₄, 1% BSA, and 0.1% NaN₃) for 1 hour, spheroplasts were labeled in PEM with the rabbit polyclonal glutathione-S-transferase (GST) antibody (1:200) for 1 hour. After thoroughly washing with PEM, cells were incubated with Alexa 488-conjugated goat anti-mouse antibody (1:1,000) for 1 hour, at RT, in the dark.

After labeled with primary and secondary antibodies, the trypanosome or yeast cells were washed and mounted on slides using Fluoromount-G mounting medium containing 5 μ g/mL of 4,6-diamidino-2-phenylindole (DAPI) to stain DNA. Differential interference contrast and fluorescence optical images were captured with a 100× objective (1.35-aperture) lens under nonsaturating conditions with an Olympus IX-71 inverted fluorescence microscope with a Photometrix CoolSnapHQ charge-coupled device camera driven by DeltaVision software (Applied Precision, Issaquah, WA). Colocalization analyses were done using FIJI software (ImageJ, National Institutes of Health, Bethesda, MD, USA) with JACoP plugin, where Pearson's correlation coefficients were obtained.

Southern blot analysis of TcPI-PLC1-KO cells

Two strategies were designed: (i) to confirm the *TcPI-PLC1* deletion and (ii) to confirm the blasticidin insertion in the *TcPI-PLC1*-KO parasites. In the first strategy, genomic DNA from WT and *TcPI-PLC1*-KO epimastigotes was isolated by phenol–chloroform extraction, digested with BamHI, separated on a 0.8% agarose gel, transferred to a nylon membrane, and hybridized with a 32 P-labeled fragment of 439 nt (*TcPI-PLC1* [nt +1 to +439] obtained by PCR (Table S1, primers 6 and 7) using the cloned *TcPI-PLC1* gene as a template and labeled using [α - 32 P]dCTP (Perkin–Elmer) with random hexanucleotide primers and the Klenow fragment of DNA polymerase (Prim-A-Gene Labeling System). Following hybridization and post-hybridization washes, detection was performed with a phosphor screen.

In the second strategy, genomic DNA from WT and *TcPl-PLC1*-KO epimastigotes was isolated by phenol–chloroform extraction, digested with Pvull, separated on a 0.8% agarose gel, transferred to a nylon membrane, and hybridized with a 32 P-labeled fragment of 430 nt (*TcPl-PLC1* [nt –503 to –1] obtained by PCR (Table S1, primers 4 and 5) using WT genomic DNA as the template and labeled using [α - 32 P]dCTP (Perkin–Elmer) with random hexanucleotide primers and the Klenow fragment of DNA polymerase (Prim-A-Gene Labeling System). Following hybridization and post-hybridization washes, detection was performed with a phosphor screen.

Southern blot analysis of TcITPK1-SKO cells

Genomic DNA from WT and *TcITPK1*-SKO epimastigotes was isolated by phenol–chloroform extraction, digested with Pvull, separated on a 0.8% agarose gel, and transferred to the nylon membrane and hybridized with a biotin-labeled fragment of 455 nt (*TcITPK1* [nt –729 to –275]) obtained by PCR (Table S1, primers 21 and 22) using WT genomic DNA as the template. The probe was labeled using the Invitrogen BioPrime DNA Labeling System kit. Hybridization was carried out in 0.5 M Na₂HPO₄, pH 7.2, and 7% SDS, at 65°C for 18 hours. Post-hybridization washes and detection were performed with the Thermo Scientific Chemiluminescent Nucleic Acid Detection Module kit, following the manufacturer's recommendations. Signal detection was performed using a ChemiDoc Imaging System (Bio-Rad).

Southern blot analysis of TcISC1-KO cells

Genomic DNA from WT and *TcISC1*-KO epimastigotes was isolated by phenol–chloroform extraction, digested with Pvull, separated on a 0.8% agarose gel, and transferred to the nylon membrane and hybridized with a biotin-labeled fragment of 435 nt (*TcISC1* [nt +694 to +1,128]) obtained by PCR (Table S1, primers 40 and 41) using the cloned *TcISC1* gene as the template. The probe was labeled using the Invitrogen BioPrime DNA Labeling System kit. Hybridization was carried out in 0.5 M Na₂HPO₄, pH 7.2, and 7% SDS, at 65°C for 18 hours. Post-hybridization washes and detection were performed with the Thermo Scientific Chemiluminescent Nucleic Acid Detection Module kit, following the manufacturer's recommendations. Signal detection was performed using a ChemiDoc Imaging System (Bio-Rad).

In vitro metacyclogenesis

We followed the protocol described by Bourguignon et al. (72) with minor modifications. Epimastigotes were obtained after 4 days of incubation in the LIT medium and submitted to a stress (incubation for 2 hours in a medium containing 190 mM NaCl, 17 mM KCl, 2 mM MgCl₂, 2 mM CaCl₂, 0.035% sodium bicarbonate, 8 mM phosphate, pH 6.9, at RT; triatome artificial urine [TAU] medium). After this stress, parasites were incubated for 96 hours in the TAU 3AAG medium (which consists of the above-described TAU medium supplemented with 10 mM L-proline, 50 mM sodium L-glutamate, 2 mM sodium L-aspartate, and 10 mM glucose). Cells in the supernatant were collected and fixed with 4% paraformaldehyde in PBS for 1 hour at RT. Cells could adhere to poly-L-lysine-coated coverslips for 20 minutes at RT. Then, cells were washed and mounted on slides using the Fluoromount-G mounting medium containing 5 μ g/mL of 2-(4-aminophenyl)-1-indole-6-carboxamidine (DAPI) to stain DNA.

In vitro infection assay

Gamma-irradiated (2,000 rad) Vero cells (4×10^5 cells) were plated onto sterile coverslips in a 12-well plate and incubated overnight at 35°C, 7% CO₂, in RPMI medium plus 10% fresh fetal bovine serum. Tissue culture-derived trypomastigote collections were incubated at 4°C overnight to allow amastigotes to settle from swimming trypomastigotes. Trypomastigotes from the supernatants of these collections were counted and used to infect the coverslips at a ratio of 50 parasites to one host cell. At 4 hours post-infection, coverslips were washed extensively with Dulbecco's Hanks' solution, followed by washing with phosphate-buffered saline (PBS), pH 7.4, to remove any extracellular parasites. Coverslips were fixed immediately in 4% paraformaldehyde in PBS, pH 7.4, at 4°C for 30 minutes. Coverslips were washed once with PBS and mounted onto glass slides in Fluoromount G containing 15 μ g/mL of 2-(4-aminophenyl)-1H-indole-6-carboxamidine (DAPI), which stains host and parasite DNA. Coverslips were viewed on an Olympus BX60 microscope to quantify the number of host cells that contained intracellular parasites and the number of intracellular parasites per cell in randomly selected fields. To quantify amastigote replication, the following modifications

were used: host cells were infected at a ratio of 10 parasites to one host cell, and coverslips were allowed to incubate for 48 hours post-infection at 35°C, 7% CO₂, prior to fixation and DAPI staining.

Inositol phosphate extraction using titanium dioxide beads followed by capillary electrophoresis electrospray ionization mass spectrometry

T. cruzi epimastigotes (1 \times 10 9 cells) were harvested and washed twice in washing buffer A with glucose (BAG; 116 mM NaCl, 5.4 mM KCl, 0.8 mM MgSO₄, 5.5 mM D-glucose, and 50 mM HEPES, pH 7.0). The pellet was then mixed with 1 M perchloric acid, resuspended by sonication (40% amplitude) for 10 seconds and kept on ice for 15 minutes. The samples were centrifuged at 18,000 \times q for 5 minutes at 4°C, and the supernatants were transferred to new tubes. Three milligrams of TiO_2 beads (Titansphere TiO_3 μm ; GL Sciences) was washed with water and 1 M perchloric acid and added to the samples and left rotating for 30 minutes at 4°C. Beads were centrifuged at 3,500 \times g, and inositol phosphates were eluted with 2.8% ammonium hydroxide. The ammonia was removed, and the samples were concentrated using a SpeedVac evaporator for 1-3 hours at 45°C. CE-ESI-MS analyses were performed on a bare-fused silica capillary with a length of 100 cm (50 µm internal diameter and 365 µm outer diameter) on an Agilent 7100 capillary electrophoresis system coupled to a Q-TOF (6520, Agilent) equipped with a commercial CE-MS adapter and sprayer kit from Agilent, as described before (24). Data were collected with Agilent OpenLAB CDS Chemstation 2.3.53 and Agilent MassHunter Workstation Acquisition for Q-TOF B.04.00.

Inositol phosphate extraction using titanium dioxide beads followed by phytase treatment

T. cruzi epimastigotes (2×10^9 cells) were harvested and washed twice in washing buffer A with glucose (BAG; 116 mM NaCl, 5.4 mM KCl, 0.8 mM MgSO₄, 5.5 mM D-glucose and 50 mM HEPES, pH 7.0). The pellet was then mixed with 1 M perchloric acid, resuspended by sonication (40% amplitude) for 10 seconds, and kept at RT for 15 minutes. The samples were centrifuged at $18,000 \times q$ for 5 minutes, and the supernatants were transferred to new tubes and boiled for 30 minutes to remove the large amount of polyphosphates present in *T. cruzi*. Five milligrams of TiO₂ beads (Titansphere TiO 5 μm; GL Sciences) was washed with water and 1 M perchloric acid and added to the sample and left rotating for 30 minutes at RT. Beads were centrifuged at 3,500 \times q, and inositol phosphates were eluted with 2.8% ammonium hydroxide. The samples were neutralized with perchloric acid and split into two. One half was digested with phytase (0.1 mg/mL) in the same medium at pH 5.0 for 1 hour at 37°C. Samples were mixed with orange G loading buffers and resolved by PAGE using 35% acrylamide/bisacrylamide 19:1 gel in Tris/borate/EDTA (TBE) buffer, as described by Losito et al. (73). Gels were stained for 30 minutes, at RT, in the toluidine blue staining solution (20% methanol; 2% glycerol; 0.05% toluidine blue) and then destained for 2 hours with several changes of the same solution without dye. Pictures were taken after exposing the gel on a white light transilluminator. Densitometric analyses were performed with ImageJ software.

Stable isotope labeling using ¹³C-glucose

Metabolic tracing experiments using 13 C-glucose were performed in the scrambled cell line (control) and TcPI-PLC1-KO mutants. For this, 100 mL of parasite cultures (initial density 2×10^6 cells/mL) was cultivated for 48 hours in the LIT medium without added D-glucose (hereafter referred to as low-glucose LIT) and supplemented with 10% FBS. After this period, samples were harvested by centrifugation (1,600 \times g for 10 minutes). Then, samples were split into two flasks. One flask was transferred to the fresh LIT medium supplemented with 5 mM 13 C-glucose and 10% FCS, while the other was supplemented with 5 mM D-glucose and 10% FCS. Both flasks were incubated for an

additional 24 hours. Subsequently, the cells were harvested by centrifugation for inositol phosphate extraction and LC-MS analysis.

Yeast transformation and culture

S. cerevisiae strains described before (17) with different genetic backgrounds: wild-type (BY4741), PLC1-ablated (plc1 Δ), and PLC1- and ISC1-ablated (plc1 Δ isc1 Δ) were incubated in 3 mL YPD media at 30°C with shaking at 200 rpm for 8 hours. Fifty microliters of the culture was inoculated in a fresh flask containing 50 mL YPD and incubated at 30°C with shaking at 200 rpm for 16–20 hours. When an OD_{600} of 0.15–0.3 was reached, yeast cells were spun down, and the supernatant was discarded. Cells were resuspended in 100 mL YPD media and incubated for 3-5 hours. Then, cells were washed once with sterile deionized water and resuspended in 3 mL 1.1× TE/LiAc solution and split between two microcentrifuge tubes. Spun-down pellets were resuspended in 600 µL 1.1× TE/LiAc solution. In a new tube, 0.1 mg salmon sperm DNA and 0.1 μg plasmid DNA (pCA45, pCA45-HsITPK1, pCA45-TcITPK1, pCA45-TcITPK1-H198A, or pCA45-TcITPK1-K242A) were mixed with 100 μL of competent yeast cells. Cells were then incubated at 30°C for 30 minutes, followed by 42°C in a water bath for 30 minutes, pelleted at 5,000 \times q, resuspended in water, and plated on selective media. After incubation at 30°C for 3-4 days, colonies were cultured in selective liquid media at 30°C overnight, harvested, and analyzed by plasmid isolation, PCR confirmation (Table S1, primers 23 and 24), and sequencing.

myo-inositol deficient growth assay

Transformed yeast cultures were grown overnight in 5 mL SC-URA media, shaking at 200 rpm, at 30°C. Yeast cultures were adjusted to $OD_{600}=10$, and 2 μ L was spotted onto SC-URA solid medium with or without myo-inositol along with four 10-fold serial dilutions. The plates were incubated at 30°C for 2–5 days and monitored every day. Each assay was repeated three times. For growth assay in liquid media, transformed yeast cultures were grown overnight in 5 mL SC-URA media, with shaking at 200 rpm, at 30°C. Yeast cultures were diluted to $OD_{600}=0.1$ in a sterile 96-well assay plate for a total volume of 200 μ L in SC-URA media or myo-inositol-deficient SC-URA media. For continued measurement of culture OD, the assay plate with lid was placed in the Synergy H1 Hybrid Multi-Mode Microplate Reader (BioTek). Yeast cultures were incubated at 30°C while shaking, and the OD_{600} was collected every 30 minutes for 40 hours. Each assay was repeated three times to achieve biological replicates.

[3H]inositol labeling, IP extraction, and SAX-HPLC analysis

The radioactive isotope labeling, IP extraction, and SAX-HPLC analysis of transformed yeasts were performed as previously described (74). In summary, yeast samples were grown overnight at 30°C in SC-URA media and then used to inoculate a fresh flask of inositol-free SC-URA media containing 5 µCi mL⁻¹ [³H]inositol. This radioactively labeled culture was grown overnight at 30°C, with shaking, to an $OD_{600} = 0.5-0.9$. Labeled yeasts were collected by centrifugation (2,000 \times g, 2 minutes, 4°C), washed once with ice-cold water or inositol-free SC-URA media, and resuspended in ice-cold water. Yeast samples were spun down $(2,000 \times q, 2 \text{ minutes}, 4^{\circ}\text{C})$ and resuspended in extraction buffer (1 M perchloric acid, 3 mM EDTA, and 0.1 mg/mL IP6) and glass beads. Yeast cell walls were broken by vortexing for 5 minutes at 4°C and debris removed by centrifugation (15,000 \times g, 5 minutes). The remaining supernatant was neutralized with neutralization buffer (1 M K₂CO₃ and 3 mM EDTA) to a pH between 6.0 and 8.0. Tubes were incubated on ice for 2 hours, flicking the mixture every 30 minutes, and then spun-down at $(15,000 \times q,$ 5 minutes). Supernatants could be stored at 4°C or immediately moved on to SAX-HPLC analysis. Yeast samples were separated onto the PartiSphere SAX (4.6 × 125 mm) column (Hichrom) and eluted with a gradient generated by mixing 1 mM EDTA and Buffer B

[1 mM EDTA/1.3 M (NH₄)₂HPO₄, pH 3.8]: 0 to 5 minutes, 0% buffer B; 5 to 10 minutes, 0 to 10% buffer B; 10 to 60 minutes, 10 to 100% buffer B; and 60 to 80 minutes, 100% buffer B. Experiments were done in triplicate.

Statistical analysis

Statistical analyses were performed with GraphPad Prism software (La Jolla, CA), version 10. Reported values are expressed as means \pm S.D of n biological experiments, as indicated in the figure legends. The level of significance was evaluated by Student's t test for comparisons between two cell lines, one-way ANOVA for comparisons between more than two cell lines, and two-way ANOVA with multiple comparison tests for analyses of grouped data.

ACKNOWLEDGMENTS

We thank Dr. Jay Bangs for providing antibodies against BiP and Dr. D. Phillips, head of the Proteomic and Mass Spectrometry (PAMS) Core Facility at UGA, for technical support in LC-MS.

This work was funded by the U.S. National Institutes of Health (NIH Grant Al173402 to R.D). M.S.B. was supported by an American Heart Association postdoctoral fellowship (AHA 24POST1196440). A.E. was supported by the NIH (T35OD010433). L.P.C. was supported by the NIH (T32Al060546). This study was supported by the German Research Foundation (DFG) under Germany's Excellence Strategy (CIBSS–EXC-2189–Project ID 390939984). H.J.J. acknowledges funding from the Volkswagen Foundation (VW Momentum Grant 98604). A.S. was supported by a Medical Research Council grant (MR/T028904/1).

AUTHOR AFFILIATIONS

¹Department of Cellular Biology, Center for Tropical and Emerging Global Diseases, University of Georgia, Athens, Georgia, USA

AUTHOR ORCIDs

Roberto Docampo http://orcid.org/0000-0003-4229-8784

FUNDING

Funder	Grant(s)	Author(s)
National Institute of Allergy and Infectious Diseases	Al173402	Roberto Docampo
American Heart Association	24POST1196440	Mayara S. Bertolini
National Institutes of Health	T35OD010433	Aharon Eidex
National Institutes of Health	T32Al060546	Logan P. Crowe
Deutsche Forschungsgemeinschaft	390939984	Henning J. Jessen
Volkswagen Foundation	98604	Henning J. Jessen
Medical Research Council	MR/T028904/1	Adolfo Saiardi

²Department of Biological Sciences, University of Cincinnati, Cincinnati, Ohio, USA

³School of Chemistry, University of Leeds, Leeds, England, United Kingdom

⁴Institute of Organic Chemistry & CIBSS-Centre for Integrative Biological Signalling Studies, University of Freiburg, Freiburg, Baden-Württemberg, Germany

⁵Medical Research Council Laboratory for Cell Biology, University College London, London, England, United Kingdom

AUTHOR CONTRIBUTIONS

Mayara S. Bertolini, Conceptualization, Data curation, Formal analysis, Funding acquisition, Investigation, Methodology, Validation, Visualization, Writing - original draft, Writing - review and editing | Sabrina E. Cline, Conceptualization, Data curation, Formal analysis, Investigation, Methodology, Software, Validation, Visualization, Writing - original draft, Writing - review and editing | Miguel A. Chiurillo, Conceptualization, Data curation, Formal analysis, Methodology, Validation, Visualization, Writing - original draft, Writing – review and editing | Brian S. Mantilla, Conceptualization, Data curation, Formal analysis, Investigation, Methodology, Validation, Writing - review and editing | Aharon Eidex, Conceptualization, Data curation, Formal analysis, Investigation, Methodology, Validation, Writing – review and editing | Logan P. Crowe, Conceptualization, Data curation, Formal analysis, Investigation, Methodology, Validation | Danye Qiu, Conceptualization, Data curation, Formal analysis, Funding acquisition, Investigation, Methodology, Resources, Supervision, Validation, Writing – review and editing | Henning J. Jessen, Conceptualization, Data curation, Formal analysis, Funding acquisition, Investigation, Methodology, Resources, Supervision, Validation, Writing - review and editing Adolfo Saiardi, Conceptualization, Data curation, Formal analysis, Funding acquisition, Investigation, Methodology, Project administration, Resources, Supervision, Validation, Writing - original draft, Writing - review and editing | Roberto Docampo, Conceptualization, Data curation, Formal analysis, Funding acquisition, Investigation, Methodology, Project administration, Resources, Supervision, Validation, Writing - original draft, Writing – review and editing

ADDITIONAL FILES

The following material is available online.

Supplemental Material

Supplemental figures (mBio03318-24-S0001.pdf). Fig. S1 to S6. Table S1 (mBio03318-24-S0002.pdf). Primers.

REFERENCES

- Gómez-Ochoa SA, Rojas LZ, Echeverría LE, Muka T, Franco OH. 2022. Global, regional, and national trends of chagas disease from 1990 to 2019: comprehensive analysis of the global burden of disease study. Glob Heart 17:59. https://doi.org/10.5334/gh.1150
- Keeling PJ, Burki F. 2019. Progress towards the tree of eukaryotes. Curr Biol 29:R808–R817. https://doi.org/10.1016/j.cub.2019.07.031
- Wilson MSC, Livermore TM, Saiardi A. 2013. Inositol pyrophosphates: between signalling and metabolism. Biochem J 452:369–379. https://doi.org/10.1042/BJ20130118
- Einicker-Lamas M, Almeida AC, Todorov AG, de Castro SL, Caruso-Neves C, Oliveira MM. 2000. Characterization of the myo-inositol transport system in trypanosoma cruzi. Eur J Biochem 267:2533–2537. https://doi. org/10.1046/j.1432-1327.2000.01302.x
- Einicker-Lamas M, Nascimento MTC, Masuda CA, Oliveira MM, Caruso-Neves C. 2007. Trypanosoma cruzi epimastigotes: regulation of myoinositol transport by effectors of protein kinases A and C. Exp Parasitol 117:171–177. https://doi.org/10.1016/j.exppara.2007.04.011
- Gonzalez-Salgado A, Steinmann ME, Greganova E, Rauch M, Mäser P, Sigel E, Bütikofer P. 2012. Myo-Inositol uptake is essential for bulk inositol phospholipid but not glycosylphosphatidylinositol synthesis in trypanosoma brucei. J Biol Chem 287:13313–13323. https://doi.org/10.1 074/jbc.M112.344812
- Drew ME, Langford CK, Klamo EM, Russell DG, Kavanaugh MP, Landfear SM. 1995. Functional expression of a myo-inositol/H+ symporter from Leishmania donovani. Mol Cell Biol 15:5508–5515. https://doi.org/10.112 8/MCB.15.10.5508
- Martin KL, Smith TK. 2006. The glycosylphosphatidylinositol (GPI) biosynthetic pathway of bloodstream-form trypanosoma brucei is dependent on the de novo synthesis of inositol. Mol Microbiol 61:89– 105. https://doi.org/10.1111/j.1365-2958.2006.05216.x

- Smith TK, Bütikofer P. 2010. Lipid metabolism in *Trypanosoma brucei*. Mol Biochem Parasitol 172:66–79. https://doi.org/10.1016/j.molbiopara. 2010.04.001
- Zhang O, Wilson MC, Xu W, Hsu F-F, Turk J, Kuhlmann FM, Wang Y, Soong L, Key P, Beverley SM, Zhang K. 2009. Degradation of host sphingomyelin is essential for *Leishmania* virulence. PLoS Pathog 5:e1000692. https://doi.org/10.1371/journal.ppat.1000692
- Zhang K, Hsu F-F, Scott DA, Docampo R, Turk J, Beverley SM. 2005. Leishmania salvage and remodelling of host sphingolipids in amastigote survival and acidocalcisome biogenesis. Mol Microbiol 55:1566–1578. ht tps://doi.org/10.1111/j.1365-2958.2005.04493.x
- Kim S, Bhandari R, Brearley CA, Saiardi A. 2024. The inositol phosphate signalling network in physiology and disease. Trends Biochem Sci 49:969–985. https://doi.org/10.1016/j.tibs.2024.08.005
- Berridge MJ. 2009. Inositol trisphosphate and calcium signalling mechanisms. Biochim Biophys Acta 1793:933–940. https://doi.org/10.10 16/j.bbamcr.2008.10.005
- Huang G, Bartlett PJ, Thomas AP, Moreno SNJ, Docampo R. 2013. Acidocalcisomes of *Trypanosoma brucei* have an inositol 1,4,5-trisphosphate receptor that is required for growth and infectivity. Proc Natl Acad Sci USA 110:1887–1892. https://doi.org/10.1073/pnas.121695
- Lander N, Chiurillo MA, Storey M, Vercesi AE, Docampo R. 2016. CRISPR/ Cas9-mediated endogenous C-terminal tagging of *Trypanosoma cruzi* genes reveals the acidocalcisome localization of the inositol 1,4,5trisphosphate receptor. J Biol Chem 291:25505–25515. https://doi.org/1 0.1074/jbc.M116.749655
- Stephens L, Radenberg T, Thiel U, Vogel G, Khoo KH, Dell A, Jackson TR, Hawkins PT, Mayr GW. 1993. The detection, purification, structural characterization, and metabolism of diphosphoinositol

pentakisphosphate(s) and bisdiphosphoinositol tetrakisphosphate(s). J Biol Chem 268:4009–4015. https://doi.org/10.1016/S0021-9258(18)5357 1-7

- Saiardi A, Azevedo C, Desfougères Y, Portela-Torres P, Wilson MSC. 2018. Microbial inositol polyphosphate metabolic pathway as drug development target. Adv Biol Regul 67:74–83. https://doi.org/10.1016/j.jbior.2017.09.007
- Cordeiro CD, Saiardi A, Docampo R. 2017. The inositol pyrophosphate synthesis pathway in *Trypanosoma brucei* is linked to polyphosphate synthesis in acidocalcisomes. Mol Microbiol 106:319–333. https://doi.org/10.1111/mmi.13766
- Mantilla BS, Amaral LDD, Jessen HJ, Docampo R. 2021. The inositol pyrophosphate biosynthetic pathway of *Trypanosoma cruzi*. ACS Chem Biol 16:283–292. https://doi.org/10.1021/acschembio.0c00759
- Potapenko E, Cordeiro CD, Huang G, Storey M, Wittwer C, Dutta AK, Jessen HJ, Starai VJ, Docampo R. 2018. 5-Diphosphoinositol pentakisphosphate (5-IP₇) regulates phosphate release from acidocalcisomes and yeast vacuoles. J Biol Chem 293:19101–19112. https://doi.org/10.10 74/jbc.RA118.005884
- Ju S, Shaltiel G, Shamir A, Agam G, Greenberg ML. 2004. Human 1-D-myo-inositol-3-phosphate synthase is functional in yeast. J Biol Chem 279:21759–21765. https://doi.org/10.1074/jbc.M312078200
- Desfougères Y, Wilson MSC, Laha D, Miller GJ, Saiardi A. 2019. ITPK1
 mediates the lipid-independent synthesis of inositol phosphates
 controlled by metabolism. Proc Natl Acad Sci USA 116:24551–24561. htt
 ps://doi.org/10.1073/pnas.1911431116
- Laha D, Parvin N, Hofer A, Giehl RFH, Fernandez-Rebollo N, von Wirén N, Saiardi A, Jessen HJ, Schaaf G. 2019. *Arabidopsis* ITPK1 and ITPK2 have an evolutionarily conserved phytic acid kinase activity. ACS Chem Biol 14:2127–2133. https://doi.org/10.1021/acschembio.9b00423
- Qiu D, Wilson MS, Eisenbeis VB, Harmel RK, Riemer E, Haas TM, Wittwer C, Jork N, Gu C, Shears SB, Schaaf G, Kammerer B, Fiedler D, Saiardi A, Jessen HJ. 2020. Analysis of inositol phosphate metabolism by capillary electrophoresis electrospray ionization mass spectrometry. Nat Commun 11:6035. https://doi.org/10.1038/s41467-020-19928-x
- Jumper J, Evans R, Pritzel A, Green T, Figurnov M, Ronneberger O, Tunyasuvunakool K, Bates R, Žídek A, Potapenko A. 2021. Highly accurate protein structure prediction with AlphaFold. Nature 596:583– 589. https://doi.org/10.1038/s41586-021-03819-2
- Roy A, Yang J, Zhang Y. 2012. COFACTOR: an accurate comparative algorithm for structure-based protein function annotation. Nucleic Acids Res 40:W471–W477. https://doi.org/10.1093/nar/gks372
- Zhang C, Freddolino PL, Zhang Y. 2017. COFACTOR: improved protein function prediction by combining structure, sequence and proteinprotein interaction information. Nucleic Acids Res 45:W291–W299. https://doi.org/10.1093/nar/gkx366
- Bliven SE, Bourne PE, Prlić A. 2015. Detection of circular permutations within protein structures using CE-CP. Bioinformatics 31:1316–1318. https://doi.org/10.1093/bioinformatics/btu823
- Li Z, Jaroszewski L, Iyer M, Sedova M, Godzik A. 2020. FATCAT 2.0: towards a better understanding of the structural diversity of proteins. Nucleic Acids Res 48:W60–W64. https://doi.org/10.1093/nar/gkaa443
- Ma J, Wang S. 2014. Algorithms, applications, and challenges of protein structure alignment. Adv Protein Chem Struct Biol 94:121–175. https://doi.org/10.1016/B978-0-12-800168-4.00005-6
- Shindyalov IN, Bourne PE. 1998. Protein structure alignment by incremental combinatorial extension (CE) of the optimal path. Protein Eng 11:739–747. https://doi.org/10.1093/protein/11.9.739
- Smith TF, Waterman MS. 1981. Identification of common molecular subsequences. J Mol Biol 147:195–197. https://doi.org/10.1016/0022-28 36(81)90087-5
- Ye Y, Godzik A. 2003. Flexible structure alignment by chaining aligned fragment pairs allowing twists. Bioinformatics 19(Suppl 2):ii246–ii255. ht tps://doi.org/10.1093/bioinformatics/btq1086
- Zhang Y, Skolnick J. 2005. TM-align: a protein structure alignment algorithm based on the TM-score. Nucleic Acids Res 33:2302–2309. https://doi.org/10.1093/nar/gki524
- Gräslund S, Sagemark J, Berglund H, Dahlgren L-G, Flores A, Hammarström M, Johansson I, Kotenyova T, Nilsson M, Nordlund P, Weigelt J. 2008. The use of systematic N- and C-terminal deletions to promote production and structural studies of recombinant proteins. Protein Expr Purif 58:210–221. https://doi.org/10.1016/j.pep.2007.11.008
- Lander N, Li Z-H, Niyogi S, Docampo R. 2015. CRISPR/Cas9-Induced disruption of paraflagellar rod protein 1 and 2 genes in *Trypanosoma*

- cruzi reveals their role in flagellar attachment. mBio 6:e01012-15. https://doi.org/10.1128/mBio.01012-15
- Chiurillo MA, Ahmed M, González C, Raja A, Lander N. 2023. Gene editing of putative cAMP and Ca²⁺ -regulated proteins using an efficient cloning-free CRISPR/Cas9 system in *Trypanosoma cruzi*. J Eukaryot Microbiol 70:e12999. https://doi.org/10.1111/jeu.12999
- Wilson MS, Saiardi A. 2018. Inositol phosphates purification using titanium dioxide beads. Bio Protoc 8:e2959. https://doi.org/10.21769/Bio Protoc.2959
- Liu G, Riemer E, Schneider R, Cabuzu D, Bonny O, Wagner CA, Qiu D, Saiardi A, Strauss A, Lahaye T, Schaaf G, Knoll T, Jessen JP, Jessen HJ. 2023. The phytase RipBL1 enables the assignment of a specific inositol phosphate isomer as a structural component of human kidney stones. RSC Chem Biol 4:300–309. https://doi.org/10.1039/d2cb00235c
- Qiu D, Gu C, Liu G, Ritter K, Eisenbeis VB, Bittner T, Gruzdev A, Seidel L, Bengsch B, Shears SB, Jessen HJ. 2023. Capillary electrophoresis mass spectrometry identifies new isomers of inositol pyrophosphates in mammalian tissues. Chem Sci 14:658–667. https://doi.org/10.1039/d2sc 05147h
- Harmel RK, Puschmann R, Nguyen Trung M, Saiardi A, Schmieder P, Fiedler D. 2019. Harnessing (13)C-labeled myo-inositol to interrogate inositol phosphate messengers by NMR. Chem Sci:5267–5274. https://doi.org/10.1039/c9sc00151d
- Laha D, Portela-Torres P, Desfougères Y, Saiardi A. 2021. Inositol phosphate kinases in the eukaryote landscape. Adv Biol Regul 79:100782. https://doi.org/10.1016/j.jbior.2020.100782
- Adl SM, Bass D, Lane CE, Lukeš J, Schoch CL, Smirnov A, Agatha S, Berney C, Brown MW, Burki F. 2019. Revisions to the classification, nomenclature, and diversity of eukaryotes. J Eukaryot Microbiol 66:4–119. https:// doi.org/10.1111/jeu.12691
- Martin KL, Smith TK. 2005. The myo-inositol-1-phosphate synthase gene is essential in *Trypanosoma brucei*. Biochem Soc Trans 33:983–985. https://doi.org/10.1042/BST0330983
- Furuya T, Kashuba C, Docampo R, Moreno SN. 2000. A novel phosphatidylinositol-phospholipase C of *Trypanosoma cruzi* that is lipid modified and activated during trypomastigote to amastigote differentiation. J Biol Chem 275:6428–6438. https://doi.org/10.1074/jbc.275.9.6428
- de Paulo Martins V, Okura M, Maric D, Engman DM, Vieira M, Docampo R, Moreno SNJ. 2010. Acylation-dependent export of *Trypanosoma cruzi* phosphoinositide-specific phospholipase C to the outer surface of amastigotes. J Biol Chem 285:30906–30917. https://doi.org/10.1074/jbc. M110.142190
- Okura M, Fang J, Salto ML, Singer RS, Docampo R, Moreno SNJ. 2005. A lipid-modified phosphoinositide-specific phospholipase C (TcPI-PLC) is involved in differentiation of trypomastigotes to amastigotes of *Trypanosoma cruzi*. J Biol Chem 280:16235–16243. https://doi.org/10.107 4/jbc.M414535200
- Martins V de P, Galizzi M, Salto ML, Docampo R, Moreno SNJ. 2010. Developmental expression of a *Trypanosoma cruzi* phosphoinositide-specific phospholipase C in amastigotes and stimulation of host phosphoinositide hydrolysis. Infect Immun 78:4206–4212. https://doi.org/10.1128/IAI.00473-10
- Szijgyarto Z, Garedew A, Azevedo C, Saiardi A. 2011. Influence of inositol pyrophosphates on cellular energy dynamics. Science 334:802–805. https://doi.org/10.1126/science.1211908
- Norman KL, Shively CA, De La Rocha AJ, Mutlu N, Basu S, Cullen PJ, Kumar A. 2018. Inositol polyphosphates regulate and predict yeast pseudohyphal growth phenotypes. PLoS Genet 14:e1007493. https://doi.org/10.1371/journal.pgen.1007493
- Kim G, Liu G, Qiu D, Gopaldass N, De Leo G, Hermes J, Timmer J, Saiardi A, Mayer A, Jessen HJ. 2024. Pools of independently cycling inositol phosphates revealed by pulse labeling with ¹⁸O-water. bioRxiv. https://d oi.org/10.1101/2024.05.03.592351
- Agusti R, Couto AS, Campetella OE, Frasch AC, de Lederkremer RM. 1997.
 The trans-sialidase of *Trypanosoma cruzi* is anchored by two different lipids. Glycobiology 7:731–735. https://doi.org/10.1093/glycob/7.6.731
- Bertello LE, Andrews NW, de Lederkremer RM. 1996. Developmentally regulated expression of ceramide in *Trypanosoma cruzi*. Mol Biochem Parasitol 79:143–151. https://doi.org/10.1016/0166-6851(96)02645-x
- 54. Serrano AA, Schenkman S, Yoshida N, Mehlert A, Richardson JM, Ferguson MA. 1995. The lipid structure of the glycosylphosphatidylinositol-anchored mucin-like sialic acid acceptors of *Trypanosoma cruzi* changes during parasite differentiation from epimastigotes to infective

- metacyclic trypomastigote forms. J Biol Chem 270:27244–27253. https://doi.org/10.1074/jbc.270.45.27244
- De Lederkremer RM, Agusti R, Docampo R. 2011. Inositolphosphoceramide metabolism in *Trypanosoma cruzi* as compared with other trypanosomatids. J Eukaryot Microbiol 58:79–87. https://doi.org/10.1111/j.1550-7408.2011.00533.x
- Alpizar-Sosa EA, Zimbres FM, Mantilla BS, Dickie EA, Wei W, Burle-Caldas GA, Filipe LNS, Van Bocxlaer K, Price HP, Ibarra-Meneses AV, Beaudry F, Fernandez-Prada C, Whitfield PD, Barrett MP, Denny PW. 2024. Evaluation of the *Leishmania* inositol phosphorylceramide synthase as a drug target using a chemical and genetic approach. ACS Infect Dis 10:2913–2928. https://doi.org/10.1021/acsinfecdis.4c00284
- Dos Santos NSA, Estevez-Castro CF, Macedo JP, Chame DF, Castro-Gomes T, Santos-Cardoso M, Burle-Caldas GA, Covington CN, Steel PG, Smith TK, Denny PW, Teixeira SMR. 2023. Disruption of the inositol phosphorylceramide synthase gene affects *Trypanosoma cruzi* differentiation and infection capacity. PLoS Negl Trop Dis 17:e0011646. https://doi.org/10.1371/journal.pntd.0011646
- Henry J, Guillotte A, Luberto C, Del Poeta M. 2011. Characterization of inositol phospho-sphingolipid-phospholipase C 1 (lsc1) in cryptococcus neoformans reveals unique biochemical features. FEBS Lett 585:635– 640. https://doi.org/10.1016/j.febslet.2011.01.015
- Zhang O, Xu W, Balakrishna Pillai A, Zhang K. 2012. Developmentally regulated sphingolipid degradation in *Leishmania* major. PLoS ONE 7:e31059. https://doi.org/10.1371/journal.pone.0031059
- Andrade LO, Andrews NW. 2004. Lysosomal fusion is essential for the retention of *Trypanosoma cruzi* inside host cells. J Exp Med 200:1135– 1143. https://doi.org/10.1084/jem.20041408
- Rego A, Cooper KF, Snider J, Hannun YA, Costa V, Côrte-Real M, Chaves SR. 2018. Acetic acid induces Sch9p-dependent translocation of lsc1p from the endoplasmic reticulum into mitochondria. Biochim Biophys Acta Mol Cell Biol Lipids 1863:576–583. https://doi.org/10.1016/j.bbalip. 2018.02.008
- Vaena de Avalos S, Okamoto Y, Hannun YA. 2004. Activation and localization of inositol phosphosphingolipid phospholipase C, Isc1p, to the mitochondria during growth of Saccharomyces cerevisiae. J Biol Chem 279:11537–11545. https://doi.org/10.1074/jbc.M309586200
- Aslett M, Aurrecoechea C, Berriman M, Brestelli J, Brunk BP, Carrington M, Depledge DP, Fischer S, Gajria B, Gao X. 2010. TriTrypDB: a functional genomic resource for the trypanosomatidae. Nucleic Acids Res 38:D457– 62. https://doi.org/10.1093/nar/gkp851

- Altschul SF, Gish W, Miller W, Myers EW, Lipman DJ. 1990. Basic local alignment search tool. J Mol Biol 215:403–410. https://doi.org/10.1016/S 0022-2836(05)80360-2
- Li L, Stoeckert CJ, Roos DS. 2003. OrthoMCL: identification of ortholog groups for eukaryotic genomes. Genome Res 13:2178–2189. https://doi. org/10.1101/gr.1224503
- Bangs JD, Uyetake L, Brickman MJ, Balber AE, Boothroyd JC. 1993.
 Molecular cloning and cellular localization of a BiP homologue in *Trypanosoma brucei*. Divergent ER retention signals in a lower eukaryote.
 J Cell Sci 105(Pt 4):1101–1113. https://doi.org/10.1242/jcs.105.4.1101
- Bone GJ, SteinertM. 1956. Isotopes incorporated in the nucleic acids of trypanosoma mega. Nature 178:308–309. https://doi.org/10.1038/17830 8a0
- Schmatz DM, Murray PK. 1982. Cultivation of *Trypanosoma cruzi* in irradiated muscle cells: improved synchronization and enhanced trypomastigote production. Parasitology 85(Pt 1):115–125. https://doi.or g/10.1017/s0031182000054202
- Moreno SN, Silva J, Vercesi AE, Docampo R. 1994. Cytosolic-free calcium elevation in *Trypanosoma cruzi* is required for cell invasion. J Exp Med 180:1535–1540. https://doi.org/10.1084/jem.180.4.1535
- Chiurillo MA, Lander N, Bertolini MS, Storey M, Vercesi AE, Docampo R. 2017. Different roles of mitochondrial calcium uniporter complex subunits in growth and infectivity of *Trypanosoma cruzi*. mBio 8:e00574-17. https://doi.org/10.1128/mBio.00574-17
- van Suylekom D, van Donselaar E, Blanchetot C, Do Ngoc LN, Humbel BM, Boonstra J. 2007. Degradation of the hexose transporter Hxt5p in Saccharomyces cerevisiae. Biol Cell 99:13–23. https://doi.org/10.1042/BC2 0060040
- Bourguignon SC, de Souza W, Souto-Padrón T. 1998. Localization of lectin-binding sites on the surface of *Trypanosoma cruzi* grown in chemically defined conditions. Histochem Cell Biol 110:527–534. https:// doi.org/10.1007/s004180050314
- Losito O, Szijgyarto Z, Resnick AC, Saiardi A. 2009. Inositol pyrophosphates and their unique metabolic complexity: analysis by gel electrophoresis. PLoS One 4:e5580. https://doi.org/10.1371/journal.pone 0005580
- Azevedo C, Saiardi A. 2006. Extraction and analysis of soluble inositol polyphosphates from yeast. Nat Protoc 1:2416–2422. https://doi.org/10. 1038/nprot.2006.337